Deletion of *TNFAIP6* Gene in Human Keratinocytes Demonstrates a Role for TSG-6 to Retain Hyaluronan Inside Epidermis

Céline Evrard[1], Emilie Faway[1], Evelyne De Vuyst[1], Olivier Svensek[1], Valérie De Glas[1], David Bergerat[2], Michel Salmon[3], Olivier De Backer[1], Bruno Flamion[1], Hélène Le-Buanec[4], Catherine Lambert de Rouvroit[1] and Yves Poumay[1]

TSG-6 is a soluble protein secreted in the extracellular matrix by various cell types in response to inflammatory stimuli. TSG-6 interacts with extracellular matrix molecules, particularly hyaluronan (HA), and promotes cutaneous wound closure in mice. Between epidermal cells, the discrete extracellular matrix contains HA and a tiny amount of TSG-6. However, challenges imposed to keratinocytes in reconstructed human epidermis revealed strong induction of TSG-6 expression, after exposure to T helper type 2 cytokines to recapitulate the atopic dermatitis phenotype or after fungal infection that causes secretion of cytokines and antimicrobial peptides. After both types of challenge, enhanced release of TSG-6 happens simultaneously with increased HA production. TSG-6 deficiency in N/TERT keratinocytes was created by inactivating *TNFAIP6* using CRISPR/Cas9. Some *TSG-6*$^{-/-}$ keratinocytes analyzed through scratch assays tend to migrate more slowly but produce reconstructed human epidermis that exhibits normal morphology and differentiation. Few significant alterations were noticed by transcriptomic analysis. Nevertheless, reduced HA content in *TSG-6*$^{-/-}$ reconstructed human epidermis was observed, along with enhanced HA release into the culture medium, and this phenotype was even more pronounced after the challenging conditions. Reintroduction of cells producing TSG-6 in reconstructed human epidermis reduced HA leakage. Our results show a role for TSG-6 in sequestering HA between epidermal cells in response to inflammation.

JID Innovations (2021);**1:**100054 doi:10.1016/j.xjidi.2021.100054

INTRODUCTION

In the skin, although occupying most of the space in the dermis, the extracellular matrix (ECM) also plays crucial roles in the epidermis, where it is composed of basal lamina and 15–20 nm intercellular spaces around cell junctions. The main ECM components in the epidermis include various polysaccharides, particularly hyaluronan (HA), which is swollen by water. This environment creates a favorable milieu for the diffusion of nutrients, GFs, and cytokines (Sandjeu and Haftek, 2009; Toole, 2001). Langerhans cells and lymphocytes migrate through the epidermal ECM, bringing innate or adaptive immunity.

HA is a linear glycosaminoglycan composed of repeated disaccharides, namely D-glucuronic acid, linked to N-acetyl-D-glucosamine, forming polymers up to 25 μm in length and 10^5–10^7 Da in mass (Sakai et al., 2000; Toole, 2004). Half of the total body HA resides in the skin (Fraser et al., 1997; Meyer and Stern, 1994), mostly in the dermis but also in the living layers of the epidermis (Pasonen-Seppänen et al., 2003). The functions of epidermal HA are not fully understood. Roles in proliferation and differentiation of epidermal keratinocytes (KCs) are unlikely, but altered regulation of HA synthases (HASs) and increased HA production were described in inflammatory conditions such as atopic dermatitis (AD) (Malaisse et al., 2014).

Across the body, HA interacts with several partners, such as TSG-6 protein, secreted by fibroblasts on TNF-α stimulation (Jadin et al., 2014; Lee et al., 1990). TSG-6 is encoded by the *TNFAIP6* gene located on human chromosome 2. The protein of 277 amino acids harbors a cleavable signal peptide, an HA-binding (LINK) domain typical of hyaladherins, and a CUB domain, typically part of ECM and plasma membrane proteins. Besides fibroblasts, several cell types secrete TSG-6 protein in response to proinflammatory stimuli (Baranova et al., 2011). Initially associated with inflammation, TSG-6 is also detected in conditions implying ECM remodeling (Fülöp et al., 2003) and in organs exerting a barrier function (Day and Milner, 2019; Tan et al., 2011). In healthy skin, TSG-6 is detected in the dermis and in living epidermal layers (Tan et al., 2011). Its expression is upregulated during skin injury (Shakya et al., 2020).

[1]*Research Unit of Molecular Physiology (URPhyM), NAmur Research Institute for LIfe Sciences (NARILIS), University of Namur, Namur, Belgium;* [2]*Inovarion SAS, Paris, France;* [3]*StratiCell, Les Isnes, Belgium; and* [4]*Laboratory of Oncodermatology, Immunology, and Cutaneous Stem Cells, National Institute of Health and Medical Research (INSERM) U976, Saint-Louis Hospital, Paris, France*

Correspondence: Yves Poumay, Research Unit of Molecular Physiology (URPhyM), NAmur Research Institute for LIfe Sciences (NARILIS), University of Namur, 61 Rue de Bruxelles, B-5000 Namur, Belgium. E-mail: yves.poumay@unamur.be

Abbreviations: AD, atopic dermatitis; crRNA, CRISPR RNA; ECM, extracellular matrix; GEO, Gene Expression Omnibus; HA, hyaluronan; HAS, hyaluronan synthase; KC, keratinocyte; KLK, kallikrein; RHE, reconstructed human epidermis; RNA-seq, RNA sequencing; Th, T helper type

Received 22 February 2021; revised 3 July 2021; accepted 12 July 2021; accepted manuscript published online XXX; corrected proof published online XXX

Cite this article as: JID Innovations 2021;1:100054

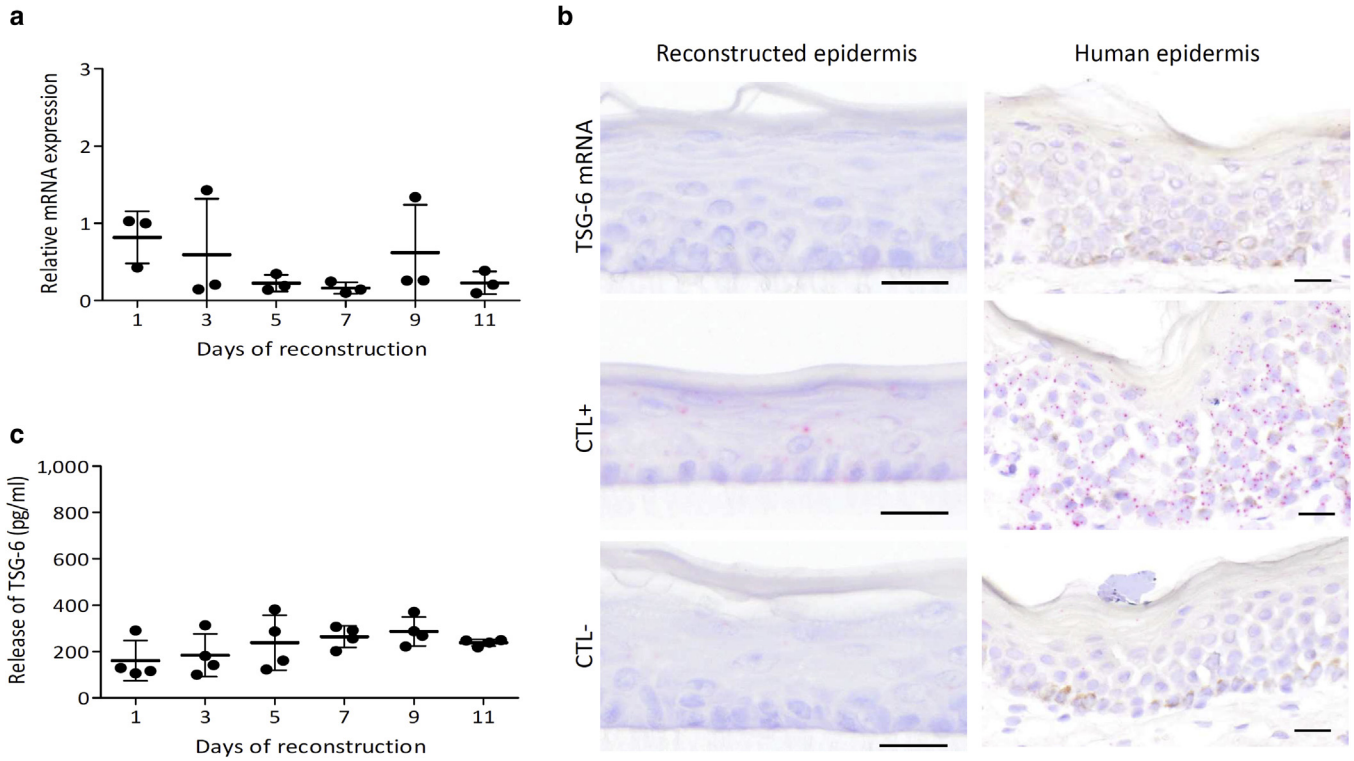

Figure 1. Weak TSG-6-encoding mRNA expression and protein release in a culture medium during the reconstruction of the normal epidermis. (**a**) TSG-6-encoding mRNA expression of RHE at 1, 3, 5, 7, 9, and 11 days of growth assessed by RT-qPCR. Reference gene is *RPLP0* (mean ± SD; n = 3; one-way ANOVA). (**b**) *TSG-6*, *PPIB* (CTL+), and *DapB* (CTL−) mRNA detection using in situ hybridization and hemalun counterstaining of day 11 RHE and normal human epidermis. Bar = 20 μm. (**c**) TSG-6 protein concentration assayed using ELISA (mean ± SD; n = 4; one-way ANOVA). CTL, control; RHE, reconstructed human epidermis.

Soluble TSG-6 protein dimerizes or interacts with ITI, and thereby becomes able to bind HA's N-acetyl glucosamine unit and favor cross-linking of HA chains in ECM (Baranova et al., 2011; Milner and Day, 2003; Milner et al., 2007). Interaction between TSG-6 and HA increases the affinity of HA for the CD44 receptor involved in KCs adhesion, proliferation, differentiation, and migration (Baranova et al., 2013; Bourguignon, 2014; Bourguignon et al., 2004; Kavasi et al., 2017; Lesley et al., 2004). CD44 also contributes to maintaining a pericellular matrix around KCs (Muto et al., 2019; Pasonen-Seppänen et al., 2012). Similar to CD44, TSG-6 holds HA in the pericellular matrix (Selbi et al., 2006), thereby controlling differentiation of, for example, fibroblasts (Simpson et al., 2009).

In this study, we investigated the human epidermis produced and challenged in vitro (Hennies and Poumay, 2021) to characterize the TSG-6 expression induced in such conditions. We then used genetic approaches to create *TSG-6*$^{-/-}$ in vitro reconstructed epidermis and analyze the potential role for TSG-6. Data show a crucial impact of TSG-6 deficiency on epidermal HA.

RESULTS

TSG-6 is expressed and released at low levels in the culture medium of normal human epidermis

Reconstructed human epidermis (RHE) produced from primary KCs (Frankart et al., 2012) was analyzed for TSG-6-encoding mRNA expression and protein release in a culture medium during the whole reconstruction process (Figure 1). RT-qPCR showed that TSG-6-encoding mRNA expression remained very low (Cq > 32). No significant induction of TSG-6-encoding mRNA was observed (Figure 1a). Accordingly, in situ hybridization was unable to detect TSG-6-encoding mRNA in normal RHE and human epidermis (Figure 1b). Secreted TSG-6 protein levels were monitored, and small amounts were detected in the culture medium during the reconstruction process (Figure 1c).

TSG-6 expression and release strongly increase on exposure of RHE to challenging conditions

To monitor TSG-6 regulation in inflammatory settings, two very different challenging conditions were imposed on RHE to analyze the tissue response.

A first challenge, mimicking AD by deprivation of plasma membrane cholesterol followed by incubation with T helper type (Th) 2 ILs and exhibiting barrier alterations (De Vuyst et al., 2018) were selected on the basis of previous transcriptomic analysis (Hubaux et al., 2018; Park et al., 2021). In response to IL-4, IL-13, and IL-25 incubation for 48 hours, *TNFAIP6* appeared as the sixth most upregulated gene, with a 27-fold increase in expression and a *P*-value of 1.37×10^{-8}. Results are accessible at Gene Expression Omnibus (GEO) Series (https://www.ncbi.nlm.nih.gov/geo/query/acc.cgi?acc=GSE149638; GSE149639). Unlike control tissues, AD-like RHE exhibited spongiosis and hypogranulosis (Figure 2a) and brighter detection of HA around KCs (Figure 2b). Analysis of TSG-6-encoding mRNA expression revealed an approximately 90-fold induction in

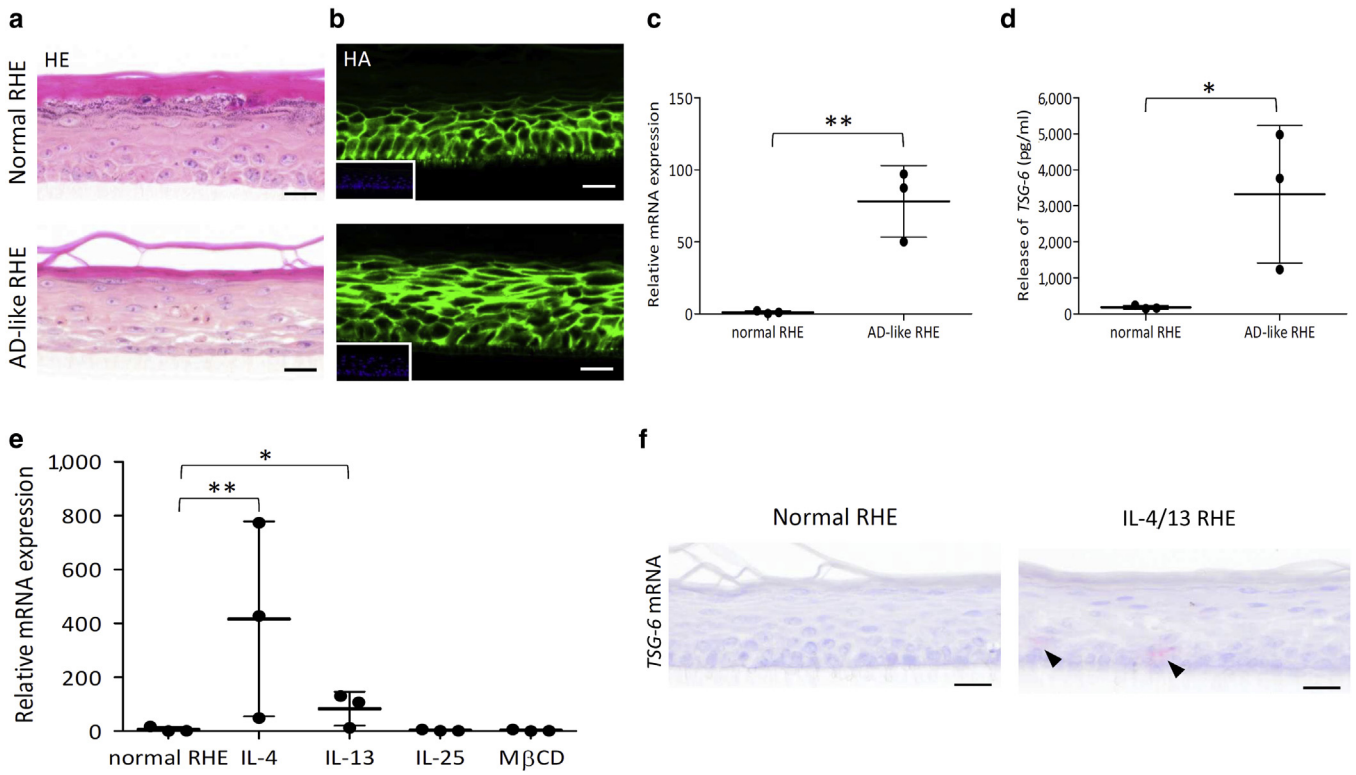

Figure 2. Increase of TSG-6-encoding mRNA and protein in challenged RHE (AD-like RHE model). RHEs were treated with MβCD and IL-4, IL-13, and IL-25 for 48 hours. (**a**) HE staining and (**b**) HA detection. Bar = 20 μm. (**c**) TSG-6-encoding mRNA expression of AD-like RHE assessed by RT-qPCR (mean ± SD; n = 3; Student *t*-test; $^{**}P < 0.01$). (**d**) TSG-6 protein concentration of challenged RHE assayed using ELISA (mean ± SD; n = 3; Student *t*-test; $^{*}P < 0.05$). (**e**) TSG-6-encoding mRNA expression of RHE treated for 48 hours by ILs or MβCD separately assessed by RT-qPCR (mean ± SD; n = 3; one-way ANOVA; $^{*}P < 0.05$; $^{**}P < 0.01$ vs. normal RHE). (**f**) *TSG-6* and *PPIB* (CTL+) mRNA detection using in situ hybridization and hemalun counterstaining of RHE challenged or not challenged with IL-4 and IL-13. AD, atopic dermatitis; HA, hyaluronan; HE, hemalun/eosin; MβCD, methyl-β-cyclodextrin; RHE, reconstructed human epidermis.

AD-like RHE compared with that of the controls (Figure 2c). The amount of TSG-6 protein released in the culture medium corroborated increased epidermal expression (Figure 2d). TSG-6-encoding mRNA expression in RHE incubated for 48 hours with either IL-4, IL-13, or IL-25 or with methyl-β-cyclodextrin identified IL-4 as the stronger inducer of TSG-6 expression, whereas IL-25 and methyl-β-cyclodextrin had no effect (Figure 2e). Thus, IL-4 and IL-13 were chosen to stimulate TSG-6 expression. In accordance with RT-qPCR data, TSG-6-encoding mRNA were detected using in situ hybridization in living layers of RHE challenged with IL-4 and IL-13 (Figure 2f**).** Conversely, addition of TNF-α in the culture medium of RHE did not induce TSG-6 expression (unpublished observations). In skin biopsies from lesional areas of patients with AD and from healthy controls, in situ hybridization was not sensitive enough to detect TSG-6-encoding mRNA (Figure 3a). However, RT-qPCR analysis of biopsies revealed increased TSG-6-encoding mRNA levels in lesional AD compared with that in the normal skin with a *P*-value as low as 0.0506 (Figure 3b). This increase in TSG-6 expression in the skin of patients suffering from AD is also detected in large-scale analyses. A search of GEO Profiles databases (Edgar et al., 2002) highlighted an increase in TSG-6 expression (GEO accession GSE5667 [Plager et al., 2010]) (Figure 3c). Likewise, transcriptomic analysis of a single-cell RNA sequencing (RNA-seq) dataset allowed a precise study of mRNA expression in undifferentiated and differentiated KCs of healthy and lesional AD skins (Reynolds et al., 2021; https://developmentcellatlas.ncl.ac.uk/datasets/ hca_skin_portal). As expected, expression of *CA2* and *NELL2*, two typical hallmarks of AD lesions, was detected in more AD KCs than in normal KCs. In parallel, TSG-6-encoding mRNA was present in some undifferentiated AD KCs, whereas the signal was barely detectable in healthy cells (Figure 3d).

A second challenge imposed on RHE consisted in superficial infection by *Trichophyton rubrum*, which induces cytokine release in concomitance with the significant induction of expression and release of TSG-6 protein (Faway et al., 2019, 2017). After 4 days of infection, RHE becomes invaded by fungal elements only in the stratum corneum (Figure 4a). At the same time, the signal of HA seems higher around the KCs of infected RHE than around the control (Figure 4b). In parallel, TSG-6-encoding mRNA can be detected through in situ hybridization solely in infected RHE (Figure 4c) when its mRNA expression is significantly increased (induction of 46-fold) according to RT-qPCR analysis. Alongside, we found an interesting significant increase in the mRNA encoding LL37, an antimicrobial peptide that blocks the proinflammatory HA–toll-like receptor 4–CD44 axis (Morioka et al., 2008) (Figure 4d).

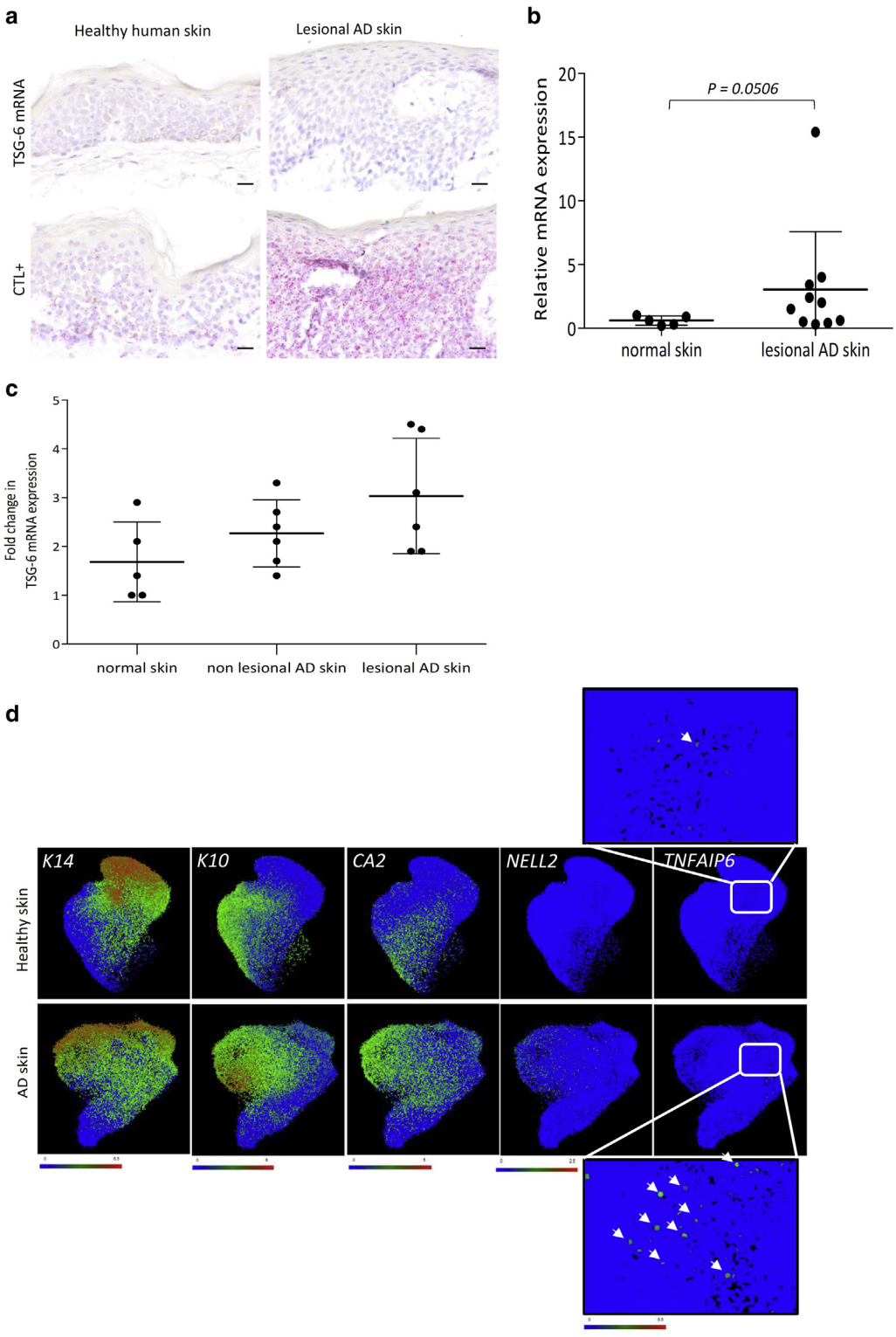

Figure 3. Increase of TSG-6-encoding mRNA in lesional AD skin. (**a**) *TSG-6* and *PPIB* (CTL+) mRNA detection using in situ hybridization and hemalun counterstaining of healthy and lesional AD skin. Bar = 20 μm. (**b**) TSG-6-encoding mRNA expression in normal and lesional AD skin assessed by RT-qPCR. The reference gene is *RPLP0* (mean ± SD; n = 5 for normal skin and n = 10 for AD skin; unpaired *t*-test with Welch's correction). (**c**) TSG-6-encoding mRNA expression in normal, nonlesional AD, and lesional AD skins analyzed from GEO Profiles database (accession GSE5667; GPL96; 206026_s_at) (mean ± SD; n = 5 or 6; one-way ANOVA). (**d**) UMAP visualization of undifferentiated and differentiated KC in healthy and lesional AD skins found in single-cell RNA-seq dataset (https://developmentcellatlas.ncl.ac.uk/datasets/ hca_skin_portal) (n = 5). Normalized gene expressions of *K14, K10, CA2, NELL2,* and *TNFAIP6* are represented in green for a low expression and in red for a strong expression. AD, atopic dermatitis; CTL, control; GEO, Gene Expression Omnibus; K, keratin; KC, keratinocyte; RNA-seq, RNA sequencing; UMAP, Uniform Manifold Approximation and Projection.

Generation, validation, and characterization of *TSG-6*$^{-/-}$ N/TERT clones

To investigate the potential roles of epidermal TSG-6, we used CRISPR/Cas9 to disrupt the *TNFAIP6* gene in N/TERT KCs. RNA-seq analysis of epidermis reconstructed from N/TERT cells and stimulated with IL-4 and IL-13 showed a transcriptional profile similar to that of AD-like models made of primary KCs (Table 1). RNA-seq data are accessible in ArrayExpress (http://www.ebi.ac.uk/arrayexpresse; E-MTAB-10095).

To generate deletions in the *TNFAIP6* gene, five targets were chosen in the first, third, and sixth exons (Figure 5a). DNA extracted from the pool of N/TERT KCs electroporated with Cas9/ribonucleoprotein was analyzed by PCR to

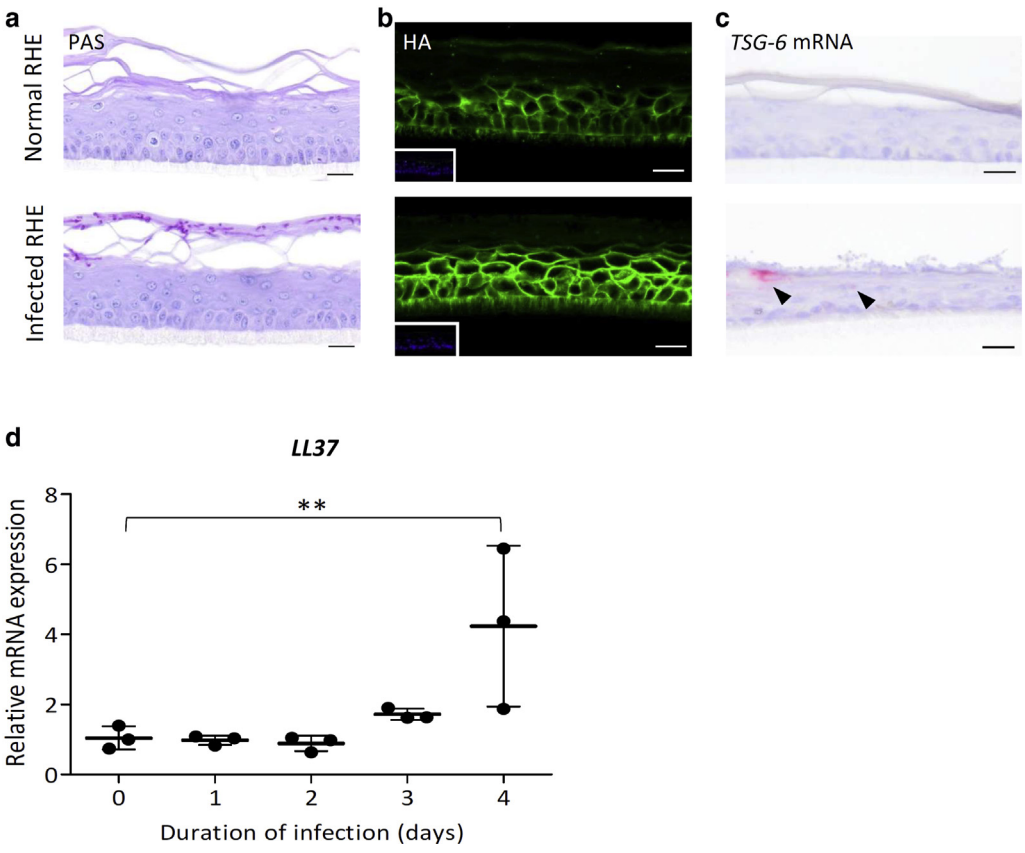

Figure 4. Elevated TSG-6-encoding mRNA expression and protein release in RHE infected by *Trichophyton rubrum* arthroconidia. RHEs were infected or not infected by *T. rubrum* arthroconidia and maintained in culture for 4 additional days. (**a**) PAS staining with α-amylase pretreatment and hemalun counterstaining and (**b**) HA detection. Bar = 20 μm. (**c**) TSG-6-encoding mRNA detection using in situ hybridization and hemalun counterstaining. Bar = 20 μm. (**d**) *LL37* mRNA expression assessed by RT-qPCR. The reference gene is *RPLP0* (mean ± SD; n = 3; one-way ANOVA; $^{**}P < 0.01$ vs. day 0). HA, hyaluronan; PAS, periodic-acid schiff; RHE, reconstructed human epidermis.

characterize deletions. Figure 5b illustrates the PCR data that revealed deletions at various sites. Among 100 clones sequenced and presenting many different mutations of several base pairs (not shown), two were selected for large deletions in both alleles of the *TNFAIP6* gene leading to probable null alleles. Genomic positions were defined by numbering nucleotide A of the methionine initiation codon as 1. The first clone *TNFAIP6*$^{UN\Delta1/UN\Delta2}$ named N/TERT *TSG-6*$^{-/-}$ *(a)* exhibits a UNΔ1 deletion in allele 1 that encompasses nucleotide −120 (i.e., 44 nucleotides upstream of exon 1) to +21,696 and a UNΔ2 deletion in allele 2 encompassing nucleotide +44 (in exon 1) to +21,635 (62 bases upstream from exon 6). The second clone *TNFAIP6*$^{UN\Delta3/UN\Delta3}$ named N/TERT *TSG-6*$^{-/-}$ *(b)* exhibits identical deletions in both alleles encompassing nucleotide +33 (in exon 1) to +21,695 (two nucleotides upstream from exon 6) (Figure 5c). Both clones encode putative peptides lacking LINK and CUB domains.

RHEs were produced using unedited *TSG-6*$^{+/+}$ or deletants *TSG-6*$^{-/-}$ *(a)* and *TSG-6*$^{-/-}$ *(b)* N/TERT cells and were treated or not treated for 48 hours with IL-4 and IL-13. Both mutant *TSG-6*$^{-/-}$ *(a)* and *TSG-6*$^{-/-}$ *(b)* clones produced RHE with a functional barrier (not shown) and exhibited identical morphological features compared with unedited N/TERT cells, including localization of keratin 10, involucrin, loricrin, and FLG (Figure 6a). As expected, TSG-6-encoding mRNA was only overexpressed in the RHE produced with *TSG-6*$^{+/+}$ N/TERT cells challenged with IL-4 and IL-13. Conversely, TSG-6-encoding mRNA was undetectable in the RHE produced with *TSG-6*$^{-/-}$ *(a)* or *TSG-6*$^{-/-}$ *(b)* N/TERT cells (Figure 6b). Using in situ hybridization, TSG-6-encoding mRNA were solely detected in living layers of *TSG-6*$^{+/+}$ N/TERT RHE challenged with IL-4 and IL-13 and were absent in knockout RHE (Figure 6c). A strong increase in TSG-6 protein level was found in the medium of challenged *TSG-6*$^{+/+}$ N/TERT but not in mutant RHE (Figure 6d). Transcriptomes of *TSG-6*$^{-/-}$ *(a)* and *TSG-6*$^{-/-}$ *(b)* RHE challenged with IL-4 and IL-13 were compared with those of *TSG-6*$^{+/+}$ RHE (http://www.ebi.ac.uk/arrayexpresse; E-MTAB-10095), confirming suppressed *TNFAIP6* expression. Deletion of TSG-6 resulted in weak upregulation and downregulation in a few genes (Table 2). Among them, suppressed expression of kallikreins (KLKs) 5 and 8, confirmed by RT-qPCR analysis in clone *TSG-6*$^{-/-}$ *(b)* (Figure 7), could indicate consequences on epidermal homeostasis and migration processes. Weak alterations in the gene expression observed after knocking out TSG-6 concurred with the normal morphology of *TSG-6*$^{-/-}$ RHE.

Deficiency in TSG-6 protein slows down KC migration

Because some genes implicated in migration (KLK5 and 8) were suppressed in *TSG-6*$^{-/-}$ RHE and because *Tsg-6*$^{-/-}$ mice show delayed wound closure (Shakya et al., 2020), the migrative ability of knocked-out TSG-6 KCs was monitored in a scratch assay. *TSG-6*$^{-/-}$ *(a)* N/TERT KCs migrated more slowly than *TSG-6*$^{+/+}$ KCs, being unable to close the scratch within 24 hours. Migration of *TSG-6*$^{-/-}$ *(b)* N/TERT KCs was also slower than that of nonedited N/TERT cells (Figure 8a). The migration defect was partially restored in the presence of recombinant TSG-6 (Figure 8b).

Table 1. Transcriptomic Analysis of Epidermis Reconstructed from N/TERT Cells and Stimulated or Not with IL-4 and IL-13 through RNA Sequencing

Gene	Name	log_2FC	P_{adj}
CISH	Cytokine inducible SH2 containing protein	3.07684025	0.000E+00
ANO1	Anoctamin 1	2.80591740	1.042E−219
SLC16A14	Solute carrier family 16 member 14	4.47550706	8.627E−192
CA2	Carbonic anhydrase 2	2.18654582	1.411E−188
CTSC	Cathepsin C	1.54462245	5.680E−123
GLDC	Glycine decarboxylase	6.48425833	7.039E−122
SLC26A2	Solute carrier family 26 member 2	1.42119675	7.896E−113
AC100801.2		2.67582484	4.386E−86
C1QTNF1	C1q and TNF related 1	2.76558625	2.474E−85
TNFAIP6	TNF alpha-induced protein 6	4.61410057	1.402E−80
BCL2L15	BCL2 like 15	4.38693821	1.861E−75
DIO_2	Iodothyronine deiodinase 2	−1.38620973	8.042E−75
ST6GAL1	ST6 beta-galactoside alpha-2,6-sialyltransferase 1	1.94904986	5.983E−73
EGR3	Early growth response 3	−1.43824080	1.248E−70
KRT16	Keratin 16	1.76615476	1.724E−67
HRH1	Histamine receptor H1	2.04522544	1.800E−60
POSTN	Periostin	2.96569063	9.221E−60
ETS2	ETS proto-oncogene 2, transcription factor	−0.97990996	3.121E−59
EGLN3	Egl-9 family hypoxia inducible factor 3	1.90222718	7.334E−58
APOL6	Apolipoprotein L6	1.11187734	1.488E−57
LBH	LBH regulator Of WNT signaling pathway	1.63185691	3.760E−57
MXRA5	Matrix remodeling associated 5	−1.75646450	7.512E−56
RGMB	Repulsive guidance molecule BMP coreceptor B	1.27097907	8.026E−56
NEK6	NIMA related kinase 6	1.46907088	4.158E−55
C1orf68	Chromosome 1 open reading frame 68	−2.17535843	5.709E−54
NELL2	Neural EGFL like 2	2.77669873	1.809E−52
PTGS2	Prostaglandin-endoperoxide synthase 2	−2.48531923	2.546E−51
GCNT3	Glucosaminyl (N-acetyl) transferase 3, mucin type	2.13974316	1.036E−50
MAP3K14	Mitogen-activated protein kinase 14	1.62240356	1.088E−50
DUOX2	Dual oxidase 2	2.12196856	3.027E−50
PADI3	Peptidyl arginine deiminase 3	1.83977015	5.216E−50
CD59	CD59 molecule (CD59 blood group)	0.75327573	1.087E−49
KRT4	Keratin 4	1.99977131	1.734E−49
BMP4	Bone morphogenetic protein 4	2.53670445	1.151E−47
BTBD3	BTB domain containing 3	0.78079374	1.162E−47
AREG	Amphiregulin	−1.47407342	7.747E−47
PDE6A	Phosphodiesterase 6A	2.22277344	1.398E−46
DENND4A	DENN domain containing 4A	0.83293501	1.443E−44
CCN1	Cellular communication network factor 1	−1.81412009	2.467E−44
SORL1	Sortilin related receptor 1	0.96862192	5.845E−44
BCL10	BCL10 immune signaling adaptor	−1.01814850	9.519E−44
RASGRP1	RAS guanyl releasing protein 1	1.15867682	1.093E−43
CXCL2	C-X-C motif chemokine ligand 2 (IL-2)	−3.20712371	7.322E−43
HBEGF	Heparin-binding EGF like growth factor	−1.92196976	1.046E−42
FLT1	Fms related receptor tyrosine kinase 1	2.52370748	1.357E−42
LGALSL	Galectin like	−0.93501839	3.556E−42
CASP14	Caspase 14	−1.20133651	6.805E−41
CTSH	Cathepsin H	−1.48572279	8.798E−40
TXN	Thioredoxin	1.09419641	2.633E−39

Abbreviations: P_{adj}, adjusted *P*; FC, fold change; RHE, reconstructed human epidermis.
List of 50 more regulated genes in IL-4– and IL-13–challenged RHE compared with nonstimulated RHE based on P_{adj}-value.

Deficiency in TSG-6 protein is responsible for enhanced leakage of HA from the epidermis

The effect of TSG-6 deficiency on the synthesis and degradation of HA as well as on HA partners (CD44 and ITIH5) was investigated at the mRNA level. No alteration in knockout tissues was observed (Figure 9). CD44 and HAS3 appeared overexpressed in both *TSG-6*$^{+/+}$ and *TSG-6*$^{-/-}$ tissues stimulated with IL-4 and IL-13, in accordance with

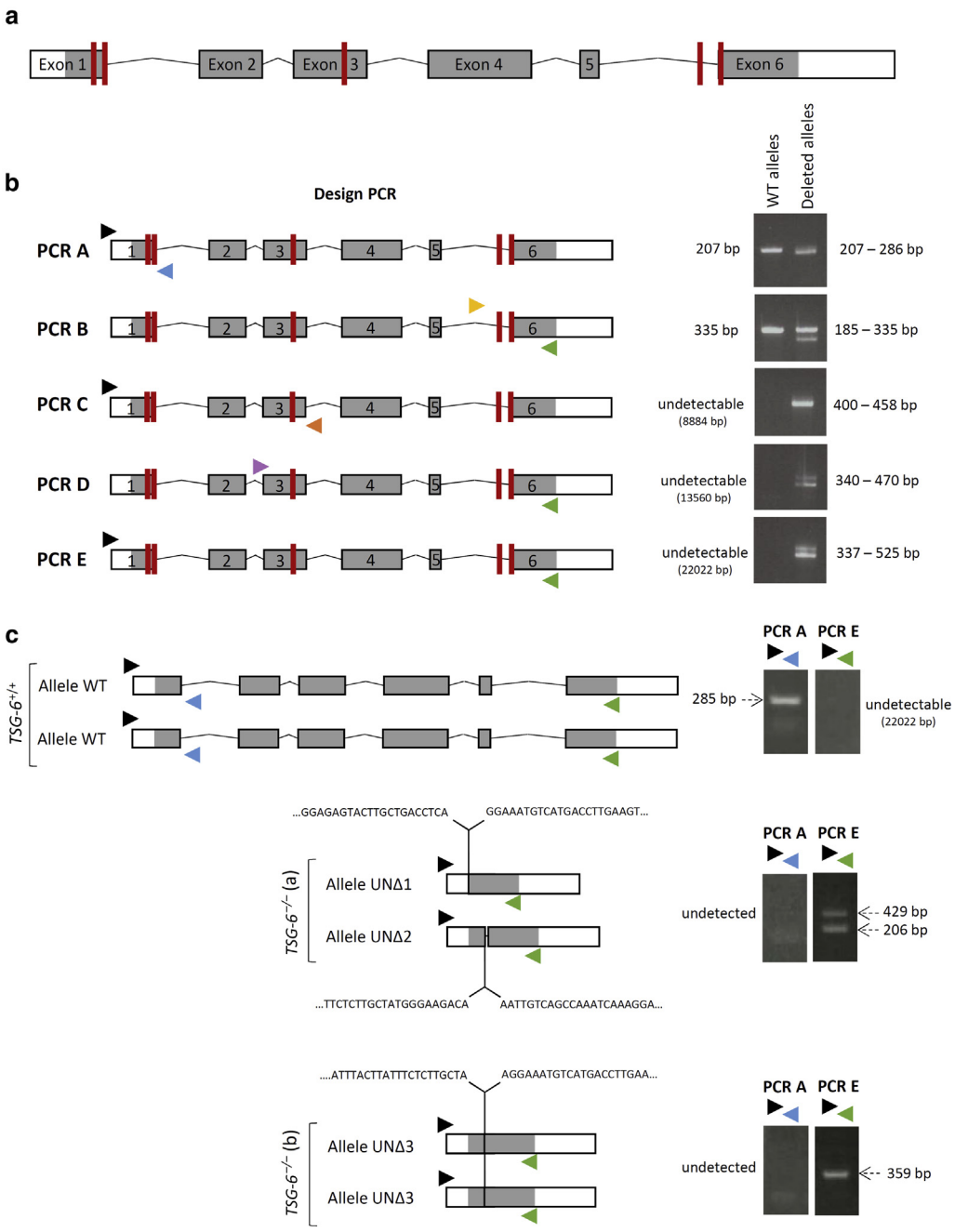

Figure 5. Deletions in *TNFAIP6* gene using CRISPR/Cas9 genome editing in N/TERT KC. (**a**) Genomic organization of *TNFAIP6* gene using the localization of five sites targeted by crRNA (red bars). (**b**) PCR screening of deletions in DNA from a pool of N/TERT cells electroporated with a mixture of five crRNA (red bars) and Cas9. Primers are indicated by arrowheads. Obtained amplicon sizes of WT and deletant alleles are shown on the right. (**c**) Genomic deletions in *TSG-6*$^{-/-}$ clone (a) and clone (b) using primer combinations PCR A and PCR E illustrated in panel b. All PCR products have been sequenced. Only the sequences of the junctions are shown. bp, base pair; crRNA, CRISPR RNA; KC, keratinocyte; WT, wild-type

previous results (De Vuyst et al., 2018; do Nascimento Pedrosa et al., 2017; Malaisse et al., 2014).

Because HAS3 is enhanced in RHE exposed to IL-4 and IL-13 and produces proinflammatory low-molecular-weight HA fragments (Weigel et al., 1997), HA released in the culture medium was analyzed using size exclusion chromatography (Figure 10). In control conditions, both *TSG-6*$^{+/+}$ and *TSG-6*$^{-/-}$ molecular-weight distribution of HA revealed similar profiles with a peak around 500 kDa (Figure 10a). When RHEs were stimulated with IL-4 and IL-13, the size of HA slightly shifted to lower molecular weights in both nonedited and knock-out tissues (Figure 10b).

Morphologically, HA distribution inside *TSG-6*$^{+/+}$ and *TSG-6*$^{-/-}$ tissues appeared similar. However, the intensity of the HA fluorescent signal was weaker in *TSG-6*$^{-/-}$ than in *TSG-6*$^{+/+}$ RHE (Figure 11a). This concurred with a larger HA amount released into the culture medium from *TSG-6*$^{-/-}$ than that from *TSG-6*$^{+/+}$ RHE, especially after IL-4 and IL-13 treatment (Figure 11b). Simultaneously, the amount of HA inside *TSG-6*$^{-/-}$ RHE was reduced, although it was nonsignificant (Figure 11c). The distribution of HA was similar in *TSG-6*$^{+/+}$ and *TSG-6*$^{-/-}$ RHE infected with dermatophytes, and HA leakage was increased from infected *TSG-6*$^{-/-}$ RHE, concomitantly with a reduced content inside tissues. However, the differences were nonsignificant (Figure 12).

To reintroduce TSG-6 in knocked-out tissues, knocked-out cells were mixed with nonedited N/TERT cells in varying proportions while reconstructing tissues (Figure 13).

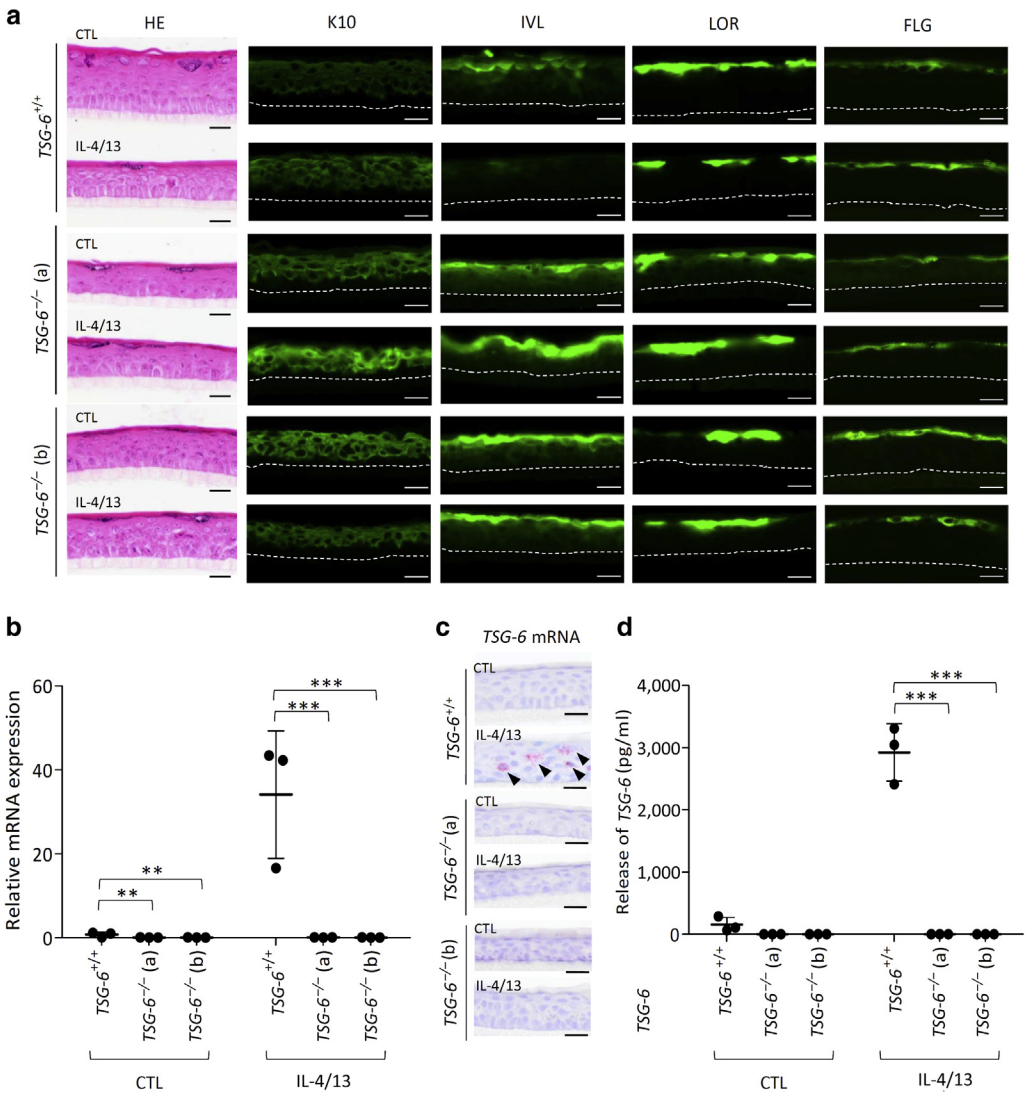

Figure 6. Validation and characterization of the two clones exhibiting large deletions in the *TNFAIP6* gene. *TSG-6*$^{+/+}$ and *TSG-6*$^{-/-}$ (a and b) RHE stimulated or not stimulated for 48 hours with IL-4 and IL-13. (**a**) HE staining and immunofluorescence (in green) of K10, IVL, LOR, and FLG. Bar = 20 μm. (**b**) TSG-6-encoding mRNA expression of *TSG-6*$^{+/+}$ and *TSG-6*$^{-/-}$ RHE assessed by RT-qPCR. The reference gene is *RPLP0* (mean ± SD; n = 3; two-way ANOVA; $^{**}P < 0.01$; $^{***}P < 0.001$ vs. *TSG-6*$^{+/+}$). (**c**) TSG-6-encoding mRNA detection using in situ hybridization and hemalun counterstaining of *TSG-6*$^{+/+}$ and *TSG-6*$^{-/-}$ RHE. Bar = 20 μm. (**d**) TSG-6 protein concentration of *TSG-6*$^{+/+}$ and *TSG-6*$^{-/-}$ RHE assayed using ELISA (mean ± SD; n = 3; two-way ANOVA; $^{***}P < 0.001$ vs. *TSG-6*$^{+/+}$). CTL, control; HE, hemalun/eosin; IVL, involucrin; K, keratin; LOR, loricrin; RHE, reconstructed human epidermis.

Interestingly, HA leakage from *TSG-6*$^{-/-}$ tissues was rescued depending on the proportion of TSG-6–producing cells (Figure 13).

For yet unidentified reason, clone *TSG-6*$^{-/-}$ *(a)* constantly releases a higher amount of HA than clone *TSG-6*$^{-/-}$ *(b)* as shown in Figures 11b and 14a despite similar expression levels of HASs and hyaluronidases (Figure 9).

In addition, pericellular HA was quantified. The RHE model does not allow to distinguish pericellular from intracellular compartment. Therefore, HA distribution was studied using monolayer cultures stimulated or not with IL-4 and IL-13 for 48 hours at the confluence. Whereas HA released in the culture medium of *TSG-6*$^{-/-}$ monolayers (Figure 14a) was increased in response to treatment, pericellular (Figure 14b) or intracellular (Figure 14c) HA was significantly reduced.

DISCUSSION

In normal conditions, TSG-6 is weakly expressed in mouse and human skin (Shakya et al., 2020; Tan et al., 2011). During in vitro reconstruction of the human epidermis, TSG-6 expression remains very weak as well.

In infected RHE, TSG-6 expression is induced in response to recognition of fungal elements by toll-like receptors, leading to production of antimicrobial peptides and cytokines such as TNF-α (Faway et al., 2019; Lee et al., 1990). TSG-6 expression is also induced in RHE exposed to Th2 cytokines to mimic typical features of AD epidermis (do Nascimento Pedrosa et al., 2017), and HA production simultaneously increases as a result of HAS3 overexpression (De Vuyst et al., 2018; Malaisse et al., 2014). In vivo, TSG-6 expression is increased in lesional AD skin and in contact dermatitis (GEO accession GSE57225 [Quaranta et al., 2014] and GEO accession GSE711996 [Tan et al., 2017]) and is upregulated in Th1/Th17 diseases such as psoriasis (GEO accession GSE166388) and wound healing (GEO accession GSE50425). Altogether, these observations show the involvement of TSG-6 in many inflammatory conditions.

To understand the role of epidermal TSG-6, deletions in the *TNFAIP6* gene were carried out by CRISPR/Cas9 in N/TERT KCs. This immortalized human cell line was chosen because it allows for proper reconstruction of epidermis able to respond to Th2 cytokines (Dickson et al., 2000; Moran et al.,

Table 2. Transcriptomic Analysis of *TSG-6*$^{-/-}$ Epidermis through RNA Sequencing

		TSG-6$^{-/-}$ (a)		TSG-6$^{-/-}$ (b)	
ID	Gene	log_2FC	P_{adj}	log_2FC	P_{adj}
ENSG00000123610	*TNFAIP6*	−7.41503	2.96E−32	−7.32736	3E−30
ENSG00000234444	*ZNF736*	−4.44636	2.81E−22	−4.69333	3.14E−18
ENSG00000170430	*MGMT*	−4.33712	8.06E−16	−4.18849	3.18E−12
ENSG00000105750	*ZNF85*	−3.87594	3.01E−37	−2.40597	9.47E−27
ENSG00000144115	*THNSL2*	−3.86052	2.91E−15	−3.78559	1.02E−13
ENSG00000187210	*GCNT1*	−3.0438	6E−50	−2.61444	6.09E−38
ENSG00000011465	*DCN*	−2.82165	1.1E−84	−1.5491	3.33E−29
ENSG00000188257	*PLA2G2A*	−2.7461	1.93E−24	−2.00917	1.94E−14
ENSG00000177990	*DPY19L2*	−2.37162	3.21E−10	−2.42415	6.58E−09
ENSG00000153802	*TMPRSS11D*	−2.35278	9.53E−15	−1.24544	0.00015
ENSG00000129455	*KLK8*	−2.27628	3.22E−18	−1.70997	1.05E−10
ENSG00000122691	*TWIST1*	−2.26396	2.75E−06	−2.35514	8.97E−08
ENSG00000103546	*SLC6A2*	−2.23051	1.73E−11	−1.01528	0.002253
ENSG00000102837	*OLFM4*	−2.10858	1.07E−09	−2.29476	3.6E−09
ENSG00000188868	*ZNF563*	−2.01096	1.75E−17	−2.394	7.67E−21
ENSG00000244242	*IFITM10*	−1.93999	6.41E−12	−1.9349	1.62E−10
ENSG00000153292	*ADGRF1*	−1.93659	6.88E−08	−1.08517	0.008469
ENSG00000206195	*DUXAP8*	−1.88083	3.76E−05	−2.0841	6.63E−07
ENSG00000213096	*ZNF254*	−1.8603	1.41E−38	−1.78	1.78E−33
ENSG00000260027	*HOXB7*	−1.72059	2.43E−05	−2.21449	1.82E−05
ENSG00000081803	*CADPS2*	−1.64989	2.05E−05	−1.67567	1.61E−05
ENSG00000237440	*AC008554.1*	−1.61936	0.000136	−2.20067	5.76E−08
ENSG00000105357	*MYH14*	−1.48954	1.63E−16	−1.0035	3.51E−07
ENSG00000101017	*CD40*	−1.47799	5.85E−06	−2.08413	1.64E−08
ENSG00000172478	*MAB21L4*	−1.44783	9.05E−36	−1.82477	1.8E−52
ENSG00000197647	*ZNF433*	−1.36208	5.15E−08	−2.48496	3.31E−17
ENSG00000167754	*KLK5*	−1.34785	2.03E−16	−1.92299	1.2E−30
ENSG00000198182	*ZNF607*	−1.344	3.92E−17	−1.09462	7.89E−11
ENSG00000250644	*AC068580.4*	−1.33136	8.21E−07	−1.14364	0.000121
ENSG00000160284	*SPATC1L*	−1.27579	0.001851	−1.65145	0.000263
ENSG00000196263	*ZNF471*	−1.20779	9.05E−05	−1.20674	0.000435
ENSG00000077063	*CTTNBP2*	−1.16597	7.2E−06	−2.10572	5.59E−12
ENSG00000235584	*AC008268.1*	−1.15826	2.67E−07	−1.34538	1.76E−08
ENSG00000091656	*ZFHX4*	−1.14386	0.00455	−1.27665	0.005149
ENSG00000196172	*ZNF681*	−1.13207	3.24E−16	−1.08222	1.35E−13
ENSG00000150687	*PRSS23*	−1.04503	8.83E−14	−1.57255	8.84E−28
ENSG00000139445	*FOXN4*	−1.03112	0.000567	−1.48352	3.45E−06
ENSG00000219665	*ZNF433-AS1*	−1.0184	0.003964	−1.37053	0.000331
ENSG00000130038	*CRACR2A*	4.155504	4.42E−37	1.339632	3.03E−05
ENSG00000007038	*PRSS21*	2.825615	4.82E−27	1.229979	3.46E−05
ENSG00000248370	*LINC02434*	2.61115	6.57E−43	1.637452	8.7E−16
ENSG00000150722	*PPP1R1C*	2.394706	1.72E−10	1.089967	0.003993
ENSG00000182389	*CACNB4*	2.179791	1.85E−23	1.175044	1.83E−06
ENSG00000131771	*PPP1R1B*	2.1777	1.76E−11	1.057933	0.004363
ENSG00000141753	*IGFBP4*	2.083609	1.45E−42	1.219661	3.22E−13
ENSG00000108176	*DNAJC12*	2.057347	2.89E−15	1.800988	4.46E−11
ENSG00000234929	*AC018685.2*	1.77764	1.76E−10	1.325183	1.51E−05
ENSG00000166897	*ELFN2*	1.660626	3.69E−06	1.268515	0.000785
ENSG00000153064	*BANK1*	1.481794	5.99E−08	1.306159	1.21E−05
ENSG00000100968	*NFATC4*	1.471711	2.94E−11	1.093399	9.51E−06
ENSG00000251003	*ZFPM2-AS1*	1.354186	3.59E−20	1.06091	2.67E−11
ENSG00000131634	*TMEM204*	1.305841	1.52E−10	2.388995	4.19E−33
ENSG00000164684	*ZNF704*	1.215393	4.55E−09	1.085985	1.47E−06
ENSG00000141622	*RNF165*	1.162247	7.5E−05	1.046022	0.001585

(*continued*)

Table 2. Continued

		TSG-6$^{-/-}$ (a)		TSG-6$^{-/-}$ (b)	
ID	Gene	log_2FC	P_{adj}	log_2FC	P_{adj}
ENSG00000179914	*ITLN1*	1.144014	0.000195	1.104532	0.001204
ENSG00000279108	*AC008537.3*	1.114701	0.001084	1.41162	0.000283
ENSG00000225968	*ELFN1*	1.04966	0.002312	1.356617	0.000548
ENSG00000172005	*MAL*	1.00604	0.000887	1.881428	3.6E−10

Abbreviations: P_{adj}, adjusted *P*; FC, fold change; RHE, reconstructed human epidermis.
List of commonly downregulated and upregulated genes in both IL-4– and IL-13–challenged *TSG-6*$^{-/-}$ RHE compared with challenged *TSG-6*$^{+/+}$ RHE (FC ≥ 2; $P < 0.01$).

2021; Rheinwald et al., 2002; Smits et al., 2017). Recently, genome editing was performed in N/TERT cells using Cas9 plasmids for studies of Harlequin ichthyosis (Enjalbert et al., 2020) to target the genes linked to glycan metabolism (Dabelsteen et al., 2020) and to knockout claudin 1 and CD40 (Moran et al., 2021). In this study, ribonucleoprotein/Cas9 complexes were preferred to plasmid to reach higher efficiency of gene editing and benefit from a lower occurrence of off targets (Farboud et al., 2018). Indeed, all analyzed N/TERT cell clones harbored mutations. Among them, two clones exhibiting major deletions that conduct to null alleles were chosen for further studies. No off-target effect was found by screening RNA-seq results.

TSG-6$^{-/-}$ KCs were used for RHE production. These tissues exhibit normal morphology in accordance with the unaltered epidermal phenotype of *Tsg-6*-knockout mice (Fülöp et al., 2003). In control and challenging conditions, deficiency of TSG-6 has no severe impact on gene expression levels as revealed by transcriptomic analysis. We noticed that the expression of decorin, a proteoglycan playing a role in cutaneous inflammatory reactions (Bocian et al., 2013), is downregulated. Of interest, KLK5 and KLK8 involved in skin homeostasis, KCs migration, and wound remodeling (Kishibe et al., 2012; Nauroy and Nyström, 2020) are also downregulated.

In the scratch assay, whereas *TSG-6*$^{-/-}$ N/TERT clone (b) shows a very discreet slowdown, the second clone (a) migrates more slowly than control cells, reminiscent of the delayed wound closure in *Tsg-6*$^{-/-}$ mouse skin (Shakya et al., 2020). The cell migration rate is partially restored by reintroduction of soluble recombinant TSG-6 in the medium, as reported with epithelial corneal cells (Lee et al., 2015).

Because the amount of HA is decreased in the pericellular matrix of *TSG-6*$^{-/-}$ KCs, we hypothesize that the defect in migration could result from poor pericellular HA organization. A disorganized ECM was described around preovulatory follicles in *Tsg-6*–knockout mice (Fülöp et al., 2003). The HA interaction with its CD44 membrane receptor is facilitated by TSG-6 (Baranova et al., 2013), and this interaction promotes HA internalization together with proliferation and migration (Bourguignon, 2014; Csoka et al., 2001; Pasonen-Seppänen et al., 2012). TSG-6 deficiency may therefore influence the HA–CD44 signaling axis and pathways located downstream of other receptors such as EGFR (Perez et al., 2013).

In *TSG-6*$^{-/-}$ RHE, a change in the localization of HA is observed. A large amount of HA diffuses into the subepidermal compartment, suggesting a role for TSG-6 in maintaining HA inside the tissue. HA leakage from the epidermis was already reported in skin equivalent models and was attributed to an improper organization of the basement membrane (Iriyama et al., 2021; Tammi et al., 2000). Nonetheless, Rosdy et al. (1993) had illustrated typical basal lamina elements in RHE. Because TSG-6 is not a constituent of the basement membrane, enhanced release of HA from

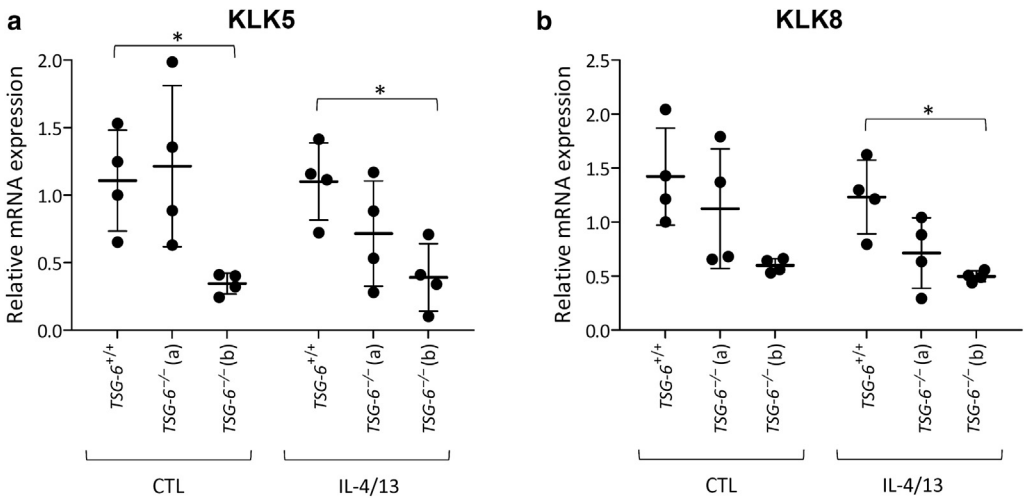

Figure 7. mRNA levels of *KLK* genes are decreased in *TSG-6*$^{-/-}$ RHE. *TSG-6*$^{+/+}$ and *TSG-6*$^{-/-}$ (a and b) RHEs were stimulated or not stimulated for 48 hours with IL-4 and IL-13. (**a**) *KLK5* and (**b**) *KLK8* mRNA expression assessed by RT-qPCR. The reference gene is *RPLP0* (mean ± SD; n = 4; two-way ANOVA; *$P < 0.05$ vs. *TSG-6*$^{+/+}$). CTL, control; KLK, kallikrein; RHE, reconstructed human epidermis.

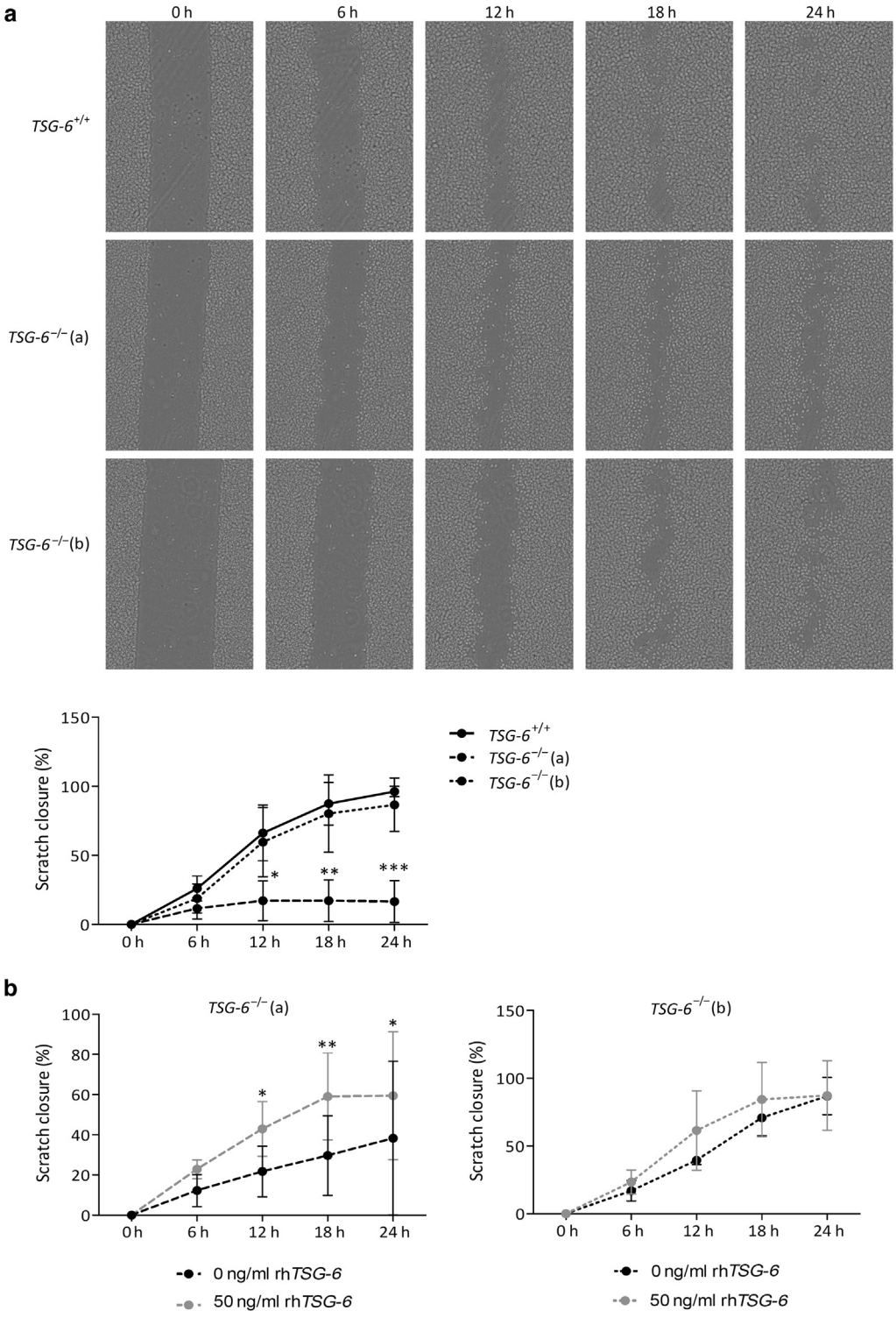

Figure 8. Lack of TSG-6 slows down KCs migration. Monolayers cultures of *TSG-6*$^{+/+}$ or *TSG-6*$^{-/-}$ (a and b) N/TERT KCs at confluence stage treated with IL-4 and IL-13 for 24 h. KCs were growth arrested by mitomycin C before performing a scratch. KCs migration was monitored for 24 h in the presence of IL-4 and IL-13. (**a**) Scratch closure was analyzed every 6 h by Cytonote and was quantified by ImageJ software (mean ± SD; n = 5; two-way ANOVA; $*P < 0.05$; $**P < 0.01$; $***P < 0.001$ vs. *TSG-6*$^{+/+}$). (**b**) Recombinant human TSG-6 protein (50 ng/ml) was added in the culture medium just after scratching monolayers cultures of *TSG-6*$^{-/-}$ (a) and (b) cells (mean ± SD; n = 3 for *TSG-6*$^{-/-}$ (a) and n = 4 for *TSG-6*$^{-/-}$ (b); two-way ANOVA; $*P < 0.05$; $**P < 0.01$ vs. 0 ng/ml rhTSG-6). Scratch closure was monitored by Cytonote and quantified by ImageJ software. h, hour; KC, keratinocyte; rhTSG-6, recombinant human TSG-6.

RHE made of *TSG-6*$^{-/-}$ cells cannot be attributed to a lack of integrity or to an altered composition of the basement membrane. We propose that the lack of HA retention in ECM is a more likely explanation.

Future studies are required to complement the data obtained with our single-cell type in vitro model. Understanding the consequences of massive HA release due to the absence of TSG-6 on underlying dermal fibroblasts and immune cells is of interest. For instance, recruitment and migration of immune cells to an inflammatory site depend on the CD44-mediated organization of HA into cables (Jokela et al., 2008; Kobayashi et al., 2020).

Our serum-free culture conditions do not allow to assess the enzymatic activity of TSG-6. Adding one source of ITI is required to investigate HA covalent cross-linking through a heavy chain. More precisely, the involvement

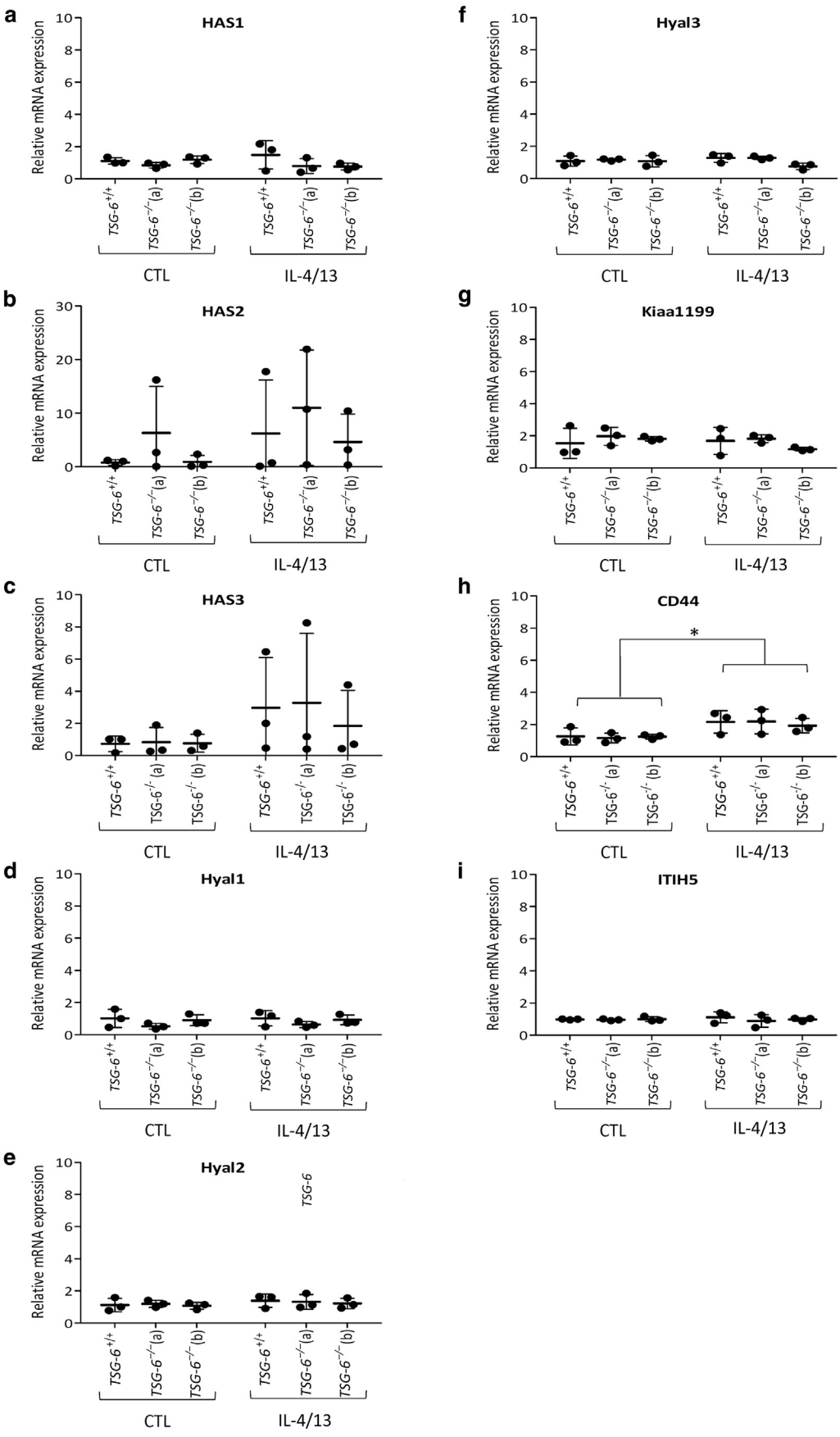

Figure 9. mRNA levels of genes related to HA are unchanged in *TSG-6*$^{-/-}$ RHE. *TSG-6*$^{+/+}$ and *TSG-6*$^{-/-}$ (a and b) RHEs were stimulated or not stimulated for 48 hours with IL-4 and IL-13. (**a**) *HAS1*, (**b**) *HAS2*, (**c**) *HAS3*, (**d**) *Hyal1*, (**e**) *Hyal2*, (**f**) *Hyal3*, (**g**) *Kiaa1199*, (**h**) *CD44*, and (**i**) *ITIH5* mRNA expression assessed by RT-qPCR. The reference gene is *RPLP0* (mean ± SD; n = 3; two-way ANOVA; **P* < 0.05). CTL, control; HA, hyaluronan; RHE, reconstructed human epidermis.

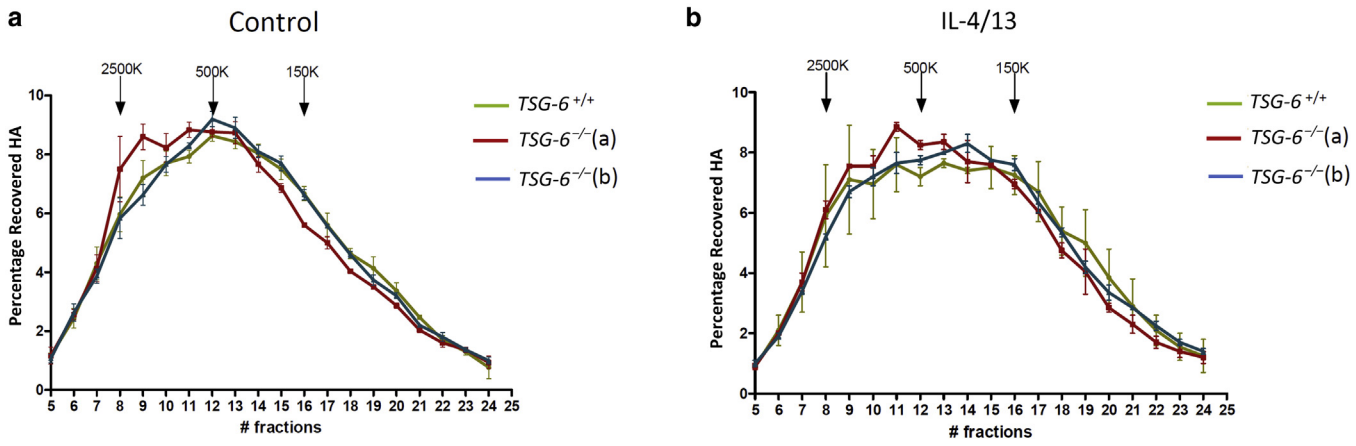

Figure 10. Similar molecular-weight distribution of HA released in the culture medium of normal and challenged *TSG-6*$^{-/-}$ RHE. The culture medium of *TSG-6*$^{+/+}$ and *TSG-6*$^{-/-}$ (a and b) RHE (**a**) control or (**b**) treated with IL-4 and IL-13 for 48 hours was collected and chromatographed on a Sephacryl S-1000 column. HA fragments of 2,500, 500, and 150 kDa were used as standards. Graphs compared HA size distribution in each fraction (mean ± SD; n = 2). #, number of; HA, hyaluronan; K, thousand; RHE, reconstructed human epidermis.

of heavy chain 5 in ECM stabilization was shown in AD and psoriasis and should therefore be further analyzed (Huth et al., 2020).

In conclusion, our data suggest a role for TSG-6 in retaining HA in inflamed epidermis by interaction and cross-linking in the ECM, as shown in other tissues (Day and Milner, 2019). In AD lesions, Th2-stimulated production of TSG-6 could participate in HA accumulation between KCs (Malaisse et al., 2014) (Figure 15). More broadly, when interacting with ECM components, TSG-6 potentially modulates the presentation of GFs and cytokines to neighboring receptors. In the epidermis, it could influence the signaling pathways related to HA (Kavasi et al., 2017) and play roles in inflammatory skin conditions.

MATERIALS AND METHODS

KCs origins, cultures, and reconstruction of the epidermis

Skin biopsies (University Hospital in Liège, Belgium) from patients with AD were collected on lesional zones as described (Mathay et al., 2011). Healthy skin biopsies and normal human KCs were isolated from abdominoplasties (Clinique St Luc, Namur, Belgium) as described (Minner et al., 2010). All samples were obtained after

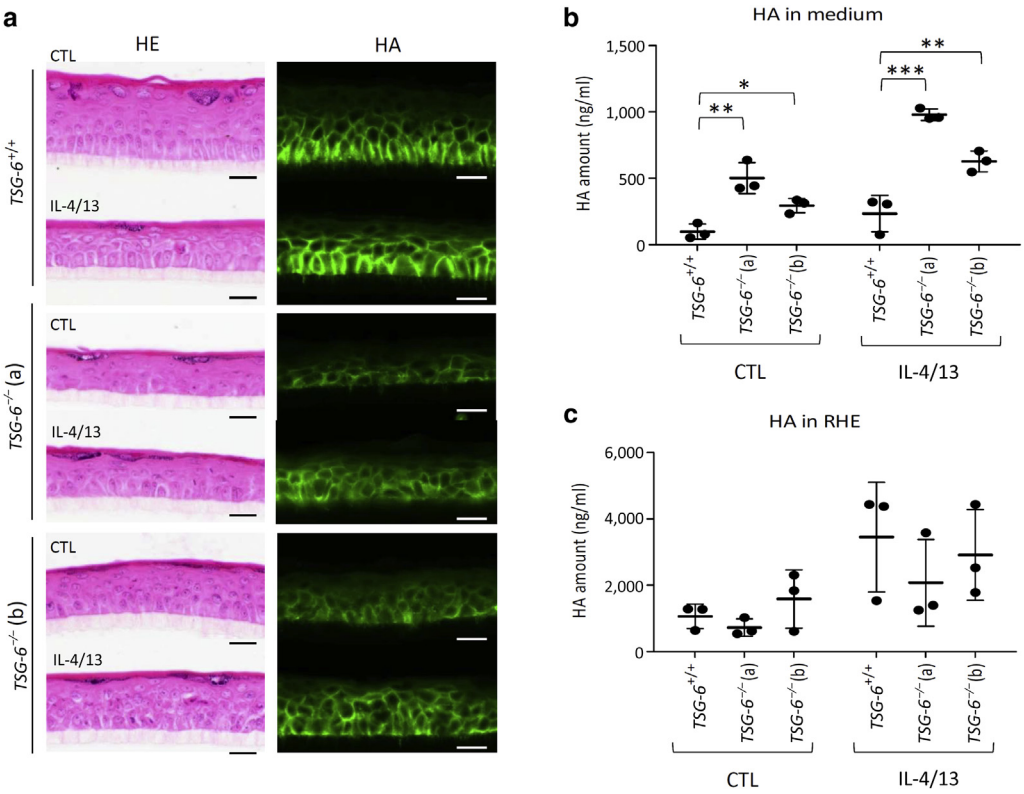

Figure 11. The change of HA localization in *TSG-6*$^{-/-}$ RHE is enhanced in Th2-challenged conditions. *TSG-6*$^{+/+}$ and TSG-6$^{-/-}$ (a and b) RHEs were stimulated or not stimulated for 48 hours with IL-4 and IL-13. (**a**) HE staining and HA detection (green). Bar = 20 μm. (**b**) HA released in culture medium measured by ELISA-like assay (mean ± SD; n = 3; two-way ANOVA; **P* < 0.05; ***P* < 0.01; ****P* < 0.001 vs. *TSG-6*$^{+/+}$). (**c**) HA remaining inside RHE (mean ± SD; n = 3; two-way ANOVA). CTL, control; HA, hyaluronan; HE, hemalun/eosin; RHE, reconstructed human epidermis; Th, T helper type.

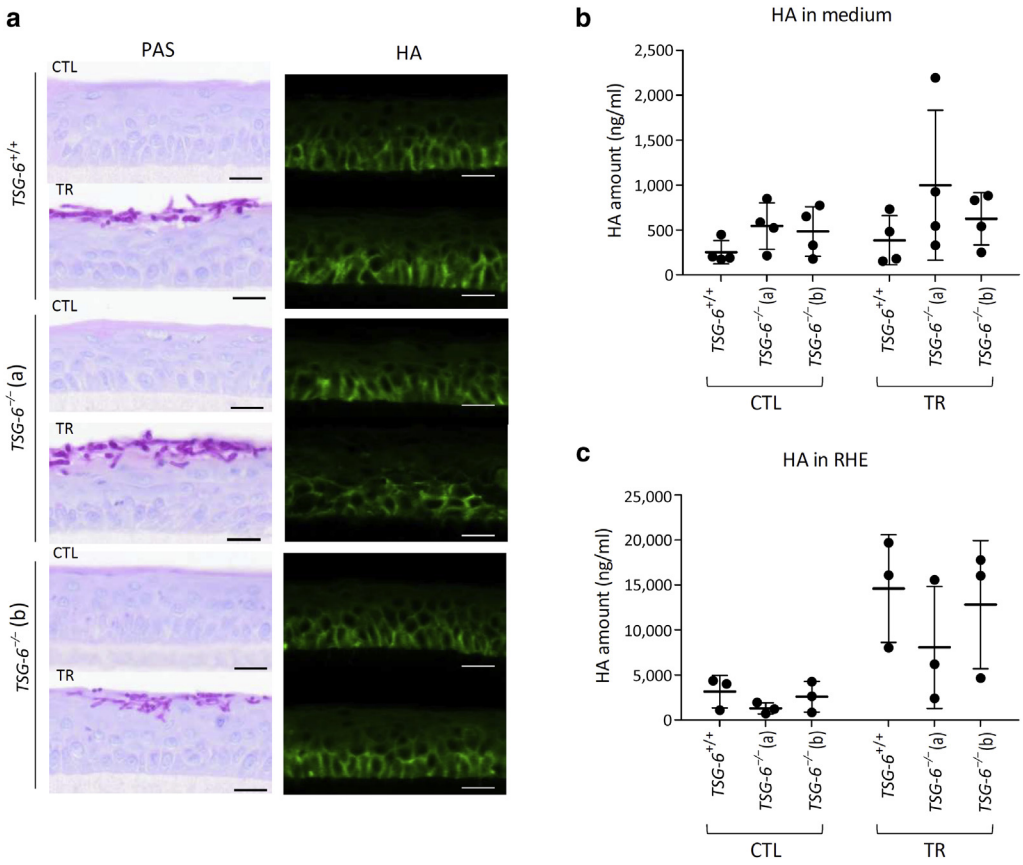

Figure 12. The change of HA localization in *TSG-6*$^{-/-}$ RHE seems to be enhanced by TR infection. *TSG-6*$^{+/+}$ and *TSG-6*$^{-/-}$ (a and b) RHE infected or not infected with TR and recovered 4 days after infection. (**a**) PAS staining with α-amylase pretreatment and hemalun counterstaining and HA detection. Bar = 20 μm. (**b**) HA released in culture medium measured by ELISA-like assay (mean ± SD; n = 4; two-way ANOVA). (**c**) HA remaining inside RHE (mean ± SD; n = 3; two-way ANOVA). CTL, control; HA, hyaluronan; PAS, periodic-acid schiff; RHE, reconstructed human epidermis; TR, *Trichophyton rubrum*.

written informed consent, in accordance with Medical Ethical Committees of the University Hospital in Liège, Clinique St-Luc in Namur, and Saint-Louis Hospital in Paris (France) and according to the Declaration of Helsinki Principles. Immortalized human KCs (N/TERT-1) were obtained from J.G. Rheinwald's laboratory (Dickson et al., 2000). Cells authenticity was assessed at ATCC

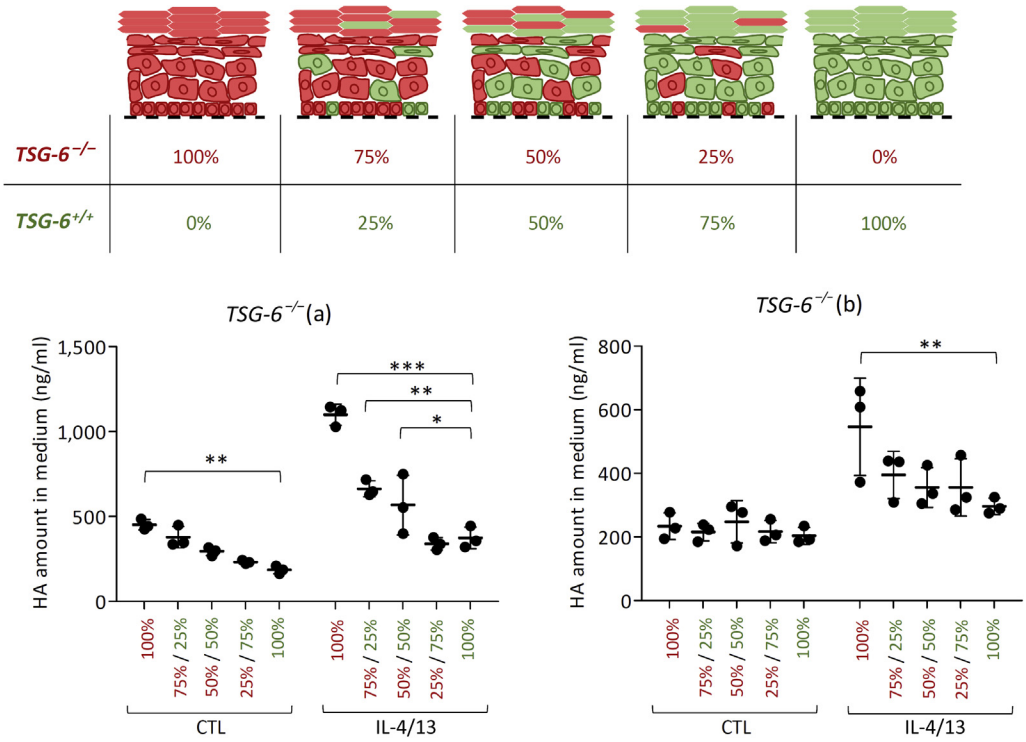

Figure 13. Introduction of *TSG-6*$^{+/+}$ cells in *TSG-6*$^{-/-}$ RHE can rescue HA leakage. Schematic representation of *TSG-6*$^{-/-}$ rescue test: epidermis were reconstructed from different ratios of *TSG-6*$^{+/+}$ (green) and *TSG-6*$^{-/-}$ (red) KCs. HA released in the culture medium of epidermis reconstructed from mixtures of KCs *TSG-6*$^{+/+}$ and *TSG-6*$^{-/-}$ (a) or *TSG-6*$^{-/-}$ (b) was measured by ELISA-like assay (mean ± SD; n = 3; two-way ANOVA; $*P < 0.05$; $**P < 0.01$; $***P < 0.001$ vs. *TSG-6*$^{+/+}$ 100%). CTL, control; HA, hyaluronan; KC, keratinocyte; RHE, reconstructed human epidermis.

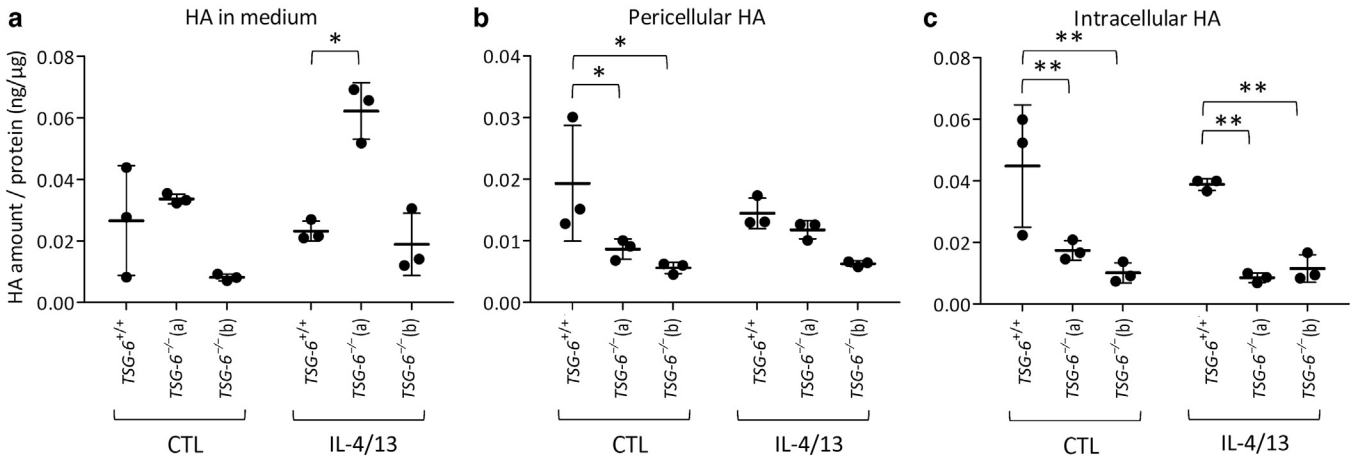

Figure 14. Change of HA localization in *TSG-6*$^{-/-}$ KCs cultured in monolayers. Autocrine monolayers cultures of *TSG-6*$^{+/+}$ or *TSG-6*$^{-/-}$ (a and b) N/TERT KCs at confluence stage treated or not treated with IL-4 and IL-13 for 48 hours. HA amount (**a**) released in the culture medium present (**b**) in pericellular spaces and (**c**) in intercellular compartment measured by ELISA-like assay and relative to the total amount of protein (mean ± SD; n = 3; two-way ANOVA; **P* < 0.05; ***P* < 0.01 vs. *TSG-6*$^{+/+}$). CTL, control; HA, hyaluronan; KC, keratinocyte.

(Manassas, VA) (http://www.atcc.org) by a comparison of an original frozen vial of cells (Bertrand-Vallery et al., 2010) with current cultured N/TERT cells. Normal and immortalized KCs were cultured as autocrine monolayer cultures (Minner et al., 2010) or were grown on a polycarbonate filter and exposed to the air–liquid interface for 11 days to produce a reconstructed epidermis (De Vuyst et al., 2014; Frankart et al., 2012). Whereas autocrine monolayers were cultured in EpiLife culture medium supplemented by amino acids (Sigma-Aldrich, St. Louis, MO) and hydrocortisone (0.18 µg/ml; Sigma-Aldrich), RHEs were grown in EpiLife medium containing Human Keratinocytes Growth Supplement (Cascade Biologics, Mansfield, United Kingdom) and calcium ion (1.5 mM), KC GF (10 ng/ml) (R&D Systems, Abingdon, United Kingdom), and vitamin C (50 mg/ml). Both cultures were maintained at 37 °C and 5% carbon dioxide.

Challenges applied to RHE to mimic AD or dermatophytosis

A described procedure was used to mimic AD alterations in RHE (De Vuyst et al., 2018). Briefly, on the 11th day of reconstruction and after cholesterol depletion with methyl-β-cyclodextrin (7.5 mM; Sigma-Aldrich, Diegem, Belgium) for 2 hours, RHEs were incubated for 48 hours with IL-4 (50 ng/ml), IL-13 (50 ng/ml), and IL-25 (20 ng/ml) (PeproTech, London, United Kingdom). RHEs were eventually challenged with IL-4 and IL-13 only for 48 hours to produce AD-like alterations in a simpler way (do Nascimento Pedrosa et al., 2017).

Another challenge was applied using infection with *T. rubrum* arthroconidia (Faway et al., 2017). Briefly, topical application of dermatophyte arthroconidia in suspension in PBS over RHE was performed on the 11th day of reconstruction. After 4 hours of exposure to these dermatophytes, RHEs were washed with PBS and then re-exposed to air for 4 additional days of culturing. This protocol was adapted for infection of RHE using N/TERT KCs. Owing to a weaker barrier, an inoculum of 850 arthroconidia per cm^2 was used instead of 1,700 per cm^2.

Scratch assay

KCs migration was studied using a scratch assay in culture (Mound et al., 2017). Confluent monolayers were treated 1 hour with 10 µg/ml mitomycin C (#sc 3514B; Santa Cruz Biotechnology, Dallas, TX) before scraping using a p200 micropipette tip and then washed and incubated with fresh medium for 24 hours. Rescue was performed by adding 50 ng/ml recombinant human TSG-6 (#2104-TS; R&D Systems) in the culture medium during the 24 hours of scratch closure. The scratch closure was monitored by time-lapse imaging using an Iprasense Cytonote device (Iprasense, Montpellier, France) and analyzed by ImageJ software (National Institutes of Health, Bethesda, MD).

Histological staining, immunofluorescence, and HA labeling

For morphological analysis, RHE and skin biopsies were fixed in a 4% formaldehyde, 70% ethanol, and 5% acetic acid solution (Lin et al., 1997) and then dehydrated and embedded in paraffin to prepare 7 µm tissue sections using a microtome. Tissue sections were stained with hemalun-eosin(-saffron). Infected RHEs were stained by periodic-acid schiff after incubation of sections with α-amylase (Faway et al., 2017).

For immunolabeling, tissue sections were incubated 1 hour at room temperature with primary anti-keratin 10 (1:100 dilution, Dako, Glostrup, Denmark), anti-involucrin (1:200 dilution, Sigma-Aldrich), and anti-loricrin (1:100 dilution, Abcam. Cambridge, United Kingdom) or overnight at 4 °C with primary anti-FLG (1:75 dilution, Thermo Fisher Scientific, Waltham, MA) antibodies and then incubated 1 hour at room temperature with secondary antibodies conjugated with Alexa fluorochrome A488: anti-mouse diluted 1:200 for keratin 10, involucrin, and FLG and anti-rabbit diluted at 1:500 for loricrin (Life Technologies, Carlsbad, CA).

HA was localized on tissue sections using an overnight incubation at 4 °C with a biotinylated HA-binding protein at 1:100 dilution (Calbiochem-Merck, Darmstadt, Germany), followed by 1-hour incubation at room temperature with fluorescein-labeled streptavidin (Vector Laboratories, Burlingame, CA).

Sections were mounted with coverslips using Mowiol (Sigma-Aldrich) and analyzed under an Olympus BX63 microscope.

RNA extraction and RT-qPCR

Total RNA was extracted using a High Pure RNA isolation kit (Roche, Basel, Switzerland) for monolayers and an RNeasy kit (Qiagen, Hilden, Germany) for RHE. First-strand cDNA was synthesized using

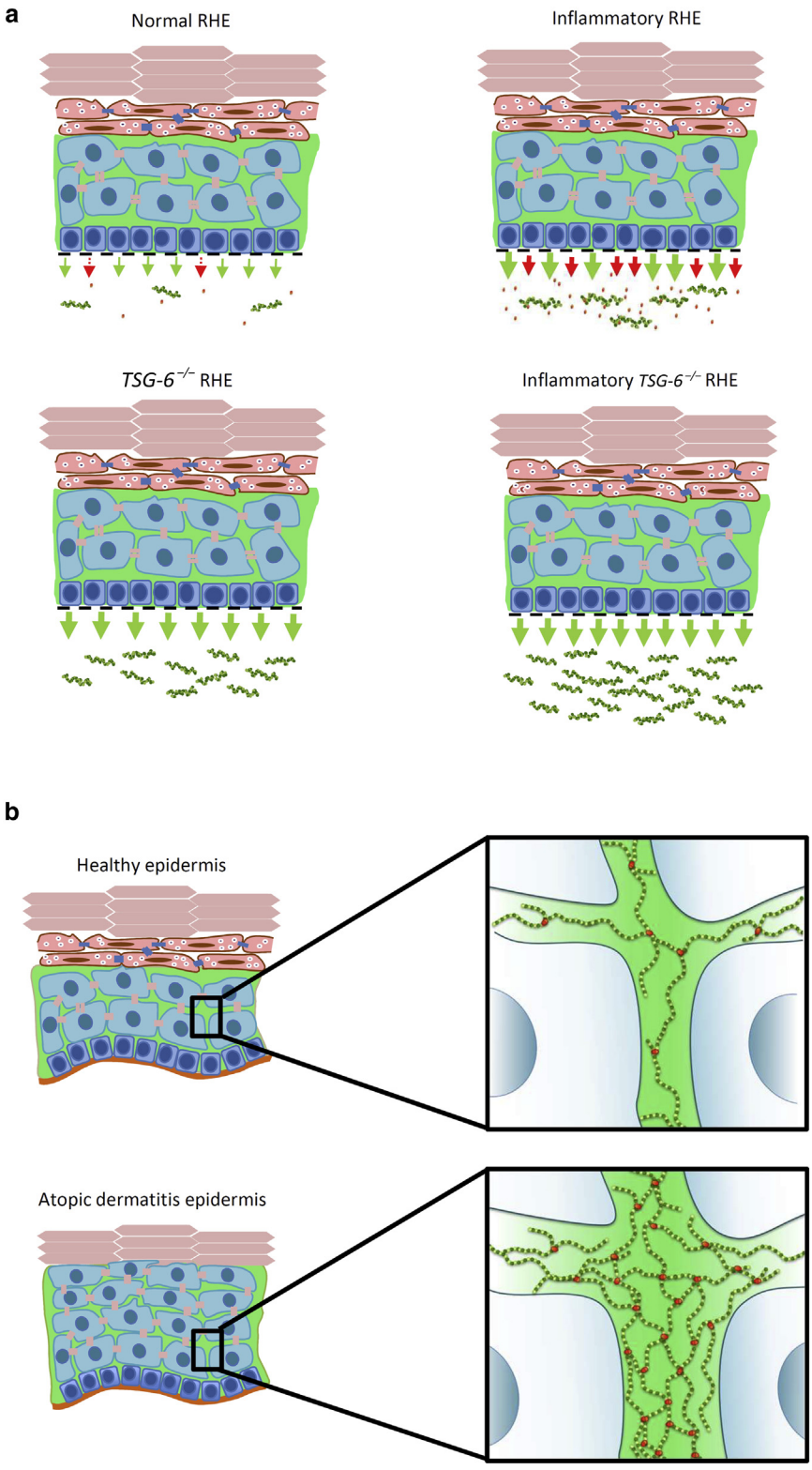

Figure 15. TSG-6 retains HA in the ECM of the epidermis. (**a**) Schematic representations of in vitro observations in *TSG-6*$^{+/+}$ and *TSG-6*$^{-/-}$ RHE challenged or not challenged. In control conditions, weak amounts of HA (green) and TSG-6 (red) are released in the culture medium. In inflammatory conditions, increased TSG-6 secretion goes along with enhanced HA release. In the absence of TSG-6, HA release is significantly increased, especially after the challenge. (**b**) Hypothetical role of TSG-6 in HA distribution and organization in healthy and lesional atopic dermatitis epidermis. In the healthy epidermis, the weak amount of secreted TSG-6 is involved in ECM organization by HA cross-linking. In atopic dermatitis lesions, enlarged intercellular spaces go along with enhanced HA production. Secreted TSG-6 links HA cables to form a dense matrix. ECM, extracellular matrix; HA, hyaluronan; RHE, reconstructed human epidermis.

SuperScript III (Invitrogen, Carlsbad, CA) and amplified by FastStart Universal SYBR Green Master (Roche) in the Light Cycler (Light Cycler 96 Instrument; Roche). Relative mRNA expression level was normalized to *RPLP0* reference gene (Minner and Poumay, 2009) and calculated using the ΔΔCq method (Livak and Schmittgen, 2001). Specifics primers (Eurogentec, Liège, Belgium) were used at 300 nM and are listed in Table 3.

RNA-seq

Total RNA was extracted using the ReliaPrep RNA Tissue Miniprep System (Promega, Madison, WI) before checking integrity through an Agilent Bioanalyzer 2100 (Agilent Technologies, Santa Clara, CA). RNA-seq and standard analysis were performed by the GIGA-Genomics platform (University of Liège, Belgium). RNA-seq data are available in the ArrayExpress database at EMBL's European

Table 3. The Sequence of Primer Pairs Used for RT-qPCR

Gene Symbol	Forward Primer	Reverse Primer
RPLP0	ATCAACGGGTACAAACGAGTC	CAGATGGATCAGCCAAGAAGG
TSG-6	GCTAGAGGCAGCCAGAAAAA	ATCCAACTCTGCCCTTAGCC
HAS1	CACCTCACCAACCGCATGCT	GTCTGCTGGCTCAGCCACCG
HAS2	CCTCATCATCCAAAGCCTGT	GATGCAAAGGGCAACTGTTT
HAS3	GCGATTCGGTGGACTACAT	GGATCCTCCTCCAGGACTC
Hyal1	TCCAGATCTTCTATGACACGACAAA	TCCTTGATGGCCTGACATGA
Hyal2	GCACTCCCAGTCTACGTCTTCA	GCACTCTCGCCAATGGTAGAG
Hyal3	GATCTGGGAGGTTCCTGTCC	AGAGCTGGAGAGGCTCAGGT
Kiaa1199	TACTGGGACGAGGACTCAGG	TCACAGCCTTTCATGGAGCA
CD44	CATTGCAGTCAACAGTCGAAGAA	ATTGCCACTGTTGATCACTAGCTT
ITIH5	ACTGTCGCTGGAGAACTGTG	CGGGGTCCTGATTTCATCGT
LL37	CCAGGACGACACAGCAGTCA	CTTCACCAGCCCGTCCTTC

Bioinformatics Institute (http://www.ebi.ac.uk/arrayexpress) under accession number E-MTAB-10095.

ELISA assay

TSG-6 protein levels were quantified in a culture medium using a homemade ELISA assay. Plates were coated overnight with an anti–TSG-6 capture antibody (#A38.1.20; Santa Cruz Biotechnology) and were blocked for 1 hour with 0.5% BSA in PBS. After 2 hours of incubation in the presence of samples of culture medium or in the presence of recombinant human TSG-6 protein (#2104-TS; R&D Systems) samples at different concentrations chosen to calibrate the assay, TSG-6 was secondarily detected using an anti–TSG-6 biotinylated antibody (#BAF2104; R&D Systems), horseradish peroxidase-streptavidin, and chromogenic substrate (R&D Systems). The concentration of TSG-6 protein is proportional to absorbance (λ: 450−570 nm) measured by spectrophotometer (Molecular Device, Berkshire, United Kingdom).

Procedures for HA analysis

The amount of HA present in the culture medium, in pericellular, and in intracellular compartments was analyzed using Hyaluronan DuoSet kit (R&D Systems) as described by Malaisse et al. (2014).

To measure the size of HA fragments, the total amount of HA recovered in the RHE culture medium was assessed using the Hyaluronan DuoSet kit. Samples were then prepared to load an identical amount of HA (10 ng of HA per sample) on a Sephacryl S-1000 column (Amersham Biosciences, Uppsala, Sweden). Samples were eluted at 70 μl/min with 0.15 M sodium acetate and 0.1% CHAPS (Sigma-Aldrich, Steinheim, Germany) to collect 30 fractions from each sample. Standard HA fragments were chromatographed in identical conditions.

In situ hybridization

RNAscope kit was used (Advanced Cell Diagnostics, Silicon Valley, CA) in accordance with the manufacturer's instructions (RNAscope 2.5 HD assay Red). Tissue sections were targeted by specific probes *Homo sapiens*-TNFAIP6 (reference 444421). *Homo sapiens*-PPIB (Peptidyl-prolyl *cis-trans* isomerase B) probe (reference 313901) was used as the positive control, and DapB (Bacillus subtilis dihydrodipicolinate reductase) probe (reference 310043) as the negative control. Fast Red staining in sections counterstained by hemalun (blue) reveals sequence hybridization as described by Wang et al. (2012).

Genome editing by CRISPR/Cas9

N/TERT KCs genome was edited to generate *TNFAIP6*-knockout cells. The procedure is a modified version of what is described in the user guide provided with the Alt-R CRISPR-Cas9 system (Integrated DNA Technologies, Coralville, IA).

Practically, CRISPR RNA (crRNA) *trans*-activating crRNA duplexes were formed by mixing crRNA (200 μM) and *trans*-activating crRNA (200 μM, #1072532; Integrated DNA Technologies), hybridizing them by heating up to 95 °C for 5 minutes, and then cooling them down to room temperature. Five crRNAs were designed using http://crispor.tefor.net/, https://zlab.bio/guide-design-resources and eu.idtdna.com website and are listed as follows: #Exon1 crRNA Up 5′-TTGCTATGGGAAGACACTCA AGG-3′, #Exon1 crRNA Down 5′-AAGGTTCTTACCAAGCCATA TGG-3′, #Exon3 crRNA Up 5′-ATT ATGGAATCCGTCTCAAT AGG-3′, #Exon6 crRNA Up 5′-GAGAAT CGACCTCTGAATTC TGG-3′, and #Exon6 crRNA Down 5′-GGTCA TGACATTTCCTGTTG GGG-3′ (Figure 5a). Duplexes were then mixed to Cas9 enzyme (#1081058; Integrated DNA Technologies) to form ribonucleoprotein complexes, which were electroporated (Amaxa Nucleofector I device, #AAD-1001; Lonza, Bâle, Switzerland) in proliferative N/TERT KCs according to the manufacturer's instructions (Amaxa Human Keratinocyte Nucleofector Kit of Lonza, #VAPD-1002). After 48 hours of recovery, edited cells were seeded in 96-well plates at low density to obtain clonal populations (limiting dilution).

The mutations in the *TNFAIP6* gene were amplified by PCR. PCR products corresponding to homologous alleles of *TSG-6* were isolated by TA cloning and sequenced by Sanger sequencing (Genewiz company, Takeley, United Kingdom). PCR primers (Eurogentec) used at 10 μM were exon 1 forward 5′-ACAGCGGAAAATGCCATTGG-3′, exon 1 reverse 5′-TCTCAACAAGAGGCTCATGAGT-3′, exon 3 forward 5′-TTGGAAGTGGCTATCTTTGCT-3′, exon 3 reverse 5′-GG AACACAACTCAATGTCGGG-3′, exon 6 forward 5′-CATGCGG-CAATGAAACCACA-3′, and exon 6 reverse 5′-AAGTGGCTAAAT CTTCCAGCT-3′ (Figure 5b).

Statistical analyses

All data were analyzed using SigmaPlot software, version 11.0 (Systat Software, Chicago, IL). Statistical differences were evaluated by Student *t*-test, one-way ANOVA, and two-way ANOVA repeated measure tests, and error bars represented SD. All graphs were performed using GraphPad Prism 5 software (GraphPad Software, San Diego, CA).

Data availability statement

Dataset related to this article can be found at https://data.mendeley.com/datasets/4fbgg2syzk/1, an open-source online data repository hosted at Mendeley Data.

ORCIDs

Céline Evrard: http://orcid.org/0000-0002-7450-0759
Emilie Faway: http://orcid.org/0000-0003-3406-1103
Evelyne De Vuyst: http://orcid.org/0000-0001-7152-1370
Olivier Svensek: http://orcid.org/0000-0001-9254-0060
Valérie De Glas: http://orcid.org/0000-0001-7366-2601
David Bergerat: http://orcid.org/0000-0003-0013-6621
Michel Salmon: http://orcid.org/0000-0002-1728-8448
Olivier De Backer: http://orcid.org/0000-0002-1490-4508
Bruno Flamion: http://orcid.org/0000-0003-4458-7627
Hélène Le-Buanec: http://orcid.org/0000-0002-2139-0357
Catherine Lambert de Rouvroit: http://orcid.org/0000-0002-0273-8995
Yves Poumay: http://orcid.org/0000-0001-5200-3367

AUTHOR CONTRIBUTIONS

Conceptualization: CE, CLDR, BF, YP; Data Curation: CE, CLDR, YP; Formal Analysis: CE; Funding Acquisition: CLDR, YP; Investigation: CE, VDG, EF, MS, DB; Methodology: CE, EF, EDV, OS, ODB, DB, HLB, CLDR, YP; Project Administration: CE, CLDR, BF, YP; Supervision: CE, CLDR, YP; Validation: CE, CLDR, YP; Visualization: CE, CLDR, YP; Writing - Original Draft Preparation: CE, CLDR, YP; Writing - Review and Editing: CE, CLDR, YP

ACKNOWLEDGMENTS

We acknowledge B. Bienfait and J.S. Blairvacq for providing skin samples and A. Nikkels for providing atopic dermatitis biopsies. We gratefully thank K. De Swert, V. Bielarz, and D. Desnoeck for their technical support; M. Caruso for the bioinformatics analyses; J. Malaisse for schemas and advice; and Marc Thiry for his skills in transmission electron microscopy analysis. EF was financially supported by the Région Wallonne (MYCEPI, convention n°1910074), and OS is a research fellow funded by FRIA (Fund for Research training in Industry and Agriculture), Belgium.

CONFLICT OF INTEREST

The authors state no conflict of interest.

REFERENCES

Baranova NS, Foulcer SJ, Briggs DC, Tilakaratna V, Enghild JJ, Milner CM, et al. Inter-α-inhibitor impairs TSG-6-induced hyaluronan cross-linking. J Biol Chem 2013;288:29642–53.

Baranova NS, Nilebäck E, Haller FM, Briggs DC, Svedhem S, Day AJ, et al. The inflammation-associated protein TSG-6 cross-links hyaluronan via hyaluronan-induced TSG-6 oligomers. J Biol Chem 2011;286:25675–86.

Bertrand-Vallery V, Boilan E, Ninane N, Demazy C, Friguet B, Toussaint O, et al. Repeated exposures to UVB induce differentiation rather than senescence of human keratinocytes lacking p16(INK-4A). Biogerontology 2010;11:167–81.

Bocian C, Urbanowitz AK, Owens RT, Iozzo RV, Götte M, Seidler DG. Decorin potentiates interferon-γ activity in a model of allergic inflammation. J Biol Chem 2013;288:12699–711.

Bourguignon LY. Matrix hyaluronan-activated CD44 signaling promotes keratinocyte activities and improves abnormal epidermal functions. Am J Pathol 2014;184:1912–9.

Bourguignon LY, Singleton PA, Diedrich F. Hyaluronan-CD44 interaction with Rac1-dependent protein kinase N-gamma promotes phospholipase Cgamma1 activation, Ca(2+) signaling, and cortactin-cytoskeleton function leading to keratinocyte adhesion and differentiation. J Biol Chem 2004;279:29654–69.

Csoka AB, Frost GI, Stern R. The six hyaluronidase-like genes in the human and mouse genomes. Matrix Biol 2001;20:499–508.

Dabelsteen S, Pallesen EMH, Marinova IN, Nielsen MI, Adamopoulou M, Rømer TB, et al. Essential functions of glycans in human epithelia dissected by a CRISPR-Cas9-Engineered human organotypic skin model. Dev Cell 2020;54:669–84.e7.

Day AJ, Milner CM. TSG-6: a multifunctional protein with anti-inflammatory and tissue-protective properties. Matrix Biol 2019;78–79:60–83.

De Vuyst E, Charlier C, Giltaire S, De Glas V, de Rouvroit CL, Poumay Y. Reconstruction of normal and pathological human epidermis on polycarbonate filter. Methods Mol Biol 2014;1195:191–201.

De Vuyst É, Giltaire S, Lambert de Rouvroit C, Malaisse J, Mound A, Bourtembourg M, et al. Methyl-β-cyclodextrin concurs with interleukin (IL)-4, IL-13 and IL-25 to induce alterations reminiscent of atopic dermatitis in reconstructed human epidermis. Exp Dermatol 2018;27:435–7.

Dickson MA, Hahn WC, Ino Y, Ronfard V, Wu JY, Weinberg RA, et al. Human keratinocytes that express hTERT and also bypass a p16(INK4a)-enforced mechanism that limits life span become immortal yet retain normal growth and differentiation characteristics. Mol Cell Biol 2000;20:1436–47.

do Nascimento Pedrosa T, De Vuyst E, Mound A, Lambert de Rouvroit C, Maria-Engler SS, Poumay Y. Methyl-β-cyclodextrin treatment combined to incubation with interleukin-4 reproduces major features of atopic dermatitis in a 3D-culture model. Arch Dermatol Res 2017;309:63–9.

Edgar R, Domrachev M, Lash AE. Gene Expression Omnibus: NCBI gene expression and hybridization array data repository. Nucleic Acids Res 2002;30:207–10.

Enjalbert F, Dewan P, Caley MP, Jones EM, Morse MA, Kelsell DP, et al. 3D model of harlequin ichthyosis reveals inflammatory therapeutic targets. J Clin Invest 2020;130:4798–810.

Farboud B, Jarvis E, Roth TL, Shin J, Corn JE, Marson A, et al. Enhanced genome editing with Cas9 ribonucleoprotein in diverse cells and organisms. J Vis Exp 2018;135:57350.

Faway E, Cambier L, De Vuyst E, Evrard C, Thiry M, Lambert de Rouvroit C, et al. Responses of reconstructed human epidermis to Trichophyton rubrum infection and impairment of infection by the inhibitor PD169316. J Invest Dermatol 2019;139:2080–9.e6.

Faway É, Cambier L, Mignon B, Poumay Y, Lambert de Rouvroit C. Modeling dermatophytosis in reconstructed human epidermis: a new tool to study infection mechanisms and to test antifungal agents. Med Mycol 2017;55:485–94.

Frankart A, Malaisse J, De Vuyst E, Minner F, de Rouvroit CL, Poumay Y. Epidermal morphogenesis during progressive in vitro 3D reconstruction at the air-liquid interface. Exp Dermatol 2012;21:871–5.

Fraser JR, Laurent TC, Laurent UB. Hyaluronan: its nature, distribution, functions and turnover. J Intern Med 1997;242:27–33.

Fülöp C, Szántó S, Mukhopadhyay D, Bárdos T, Kamath RV, Rugg MS, et al. Impaired cumulus mucification and female sterility in tumor necrosis factor-induced protein-6 deficient mice. Development 2003;130:2253–61.

Hennies HC, Poumay Y. Skin disease models in vitro and inflammatory mechanisms: predictability for drug development. Handb Exp Pharmacol 2021;265:187–218.

Hubaux R, Bastin C, Salmon M. On the relevance of an in vitro reconstructed human epidermis model for drug screening in atopic dermatitis. Exp Dermatol 2018;27:1403–7.

Huth S, Huth L, Marquardt Y, Fietkau K, Dahl E, Esser PR, et al. Inter-alpha-trypsin inhibitor heavy chain 5 (ITIH5) is a natural stabilizer of hyaluronan that modulates biological processes in the skin. Skin Pharmacol Physiol 2020;33:198–206.

Iriyama S, Nishikawa S, Hosoi J, Amano S. Basement membrane helps maintain epidermal hyaluronan content. Am J Pathol 2021;191:1010–9.

Jadin L, Huang L, Wei G, Zhao Q, Gelb AB, Frost GI, et al. Characterization of a novel recombinant hyaluronan binding protein for tissue hyaluronan detection. J Histochem Cytochem 2014;62:672–83.

Jokela TA, Lindgren A, Rilla K, Maytin E, Hascall VC, Tammi RH, et al. Induction of hyaluronan cables and monocyte adherence in epidermal keratinocytes. Connect Tissue Res 2008;49:115–9.

Kavasi RM, Berdiaki A, Spyridaki I, Corsini E, Tsatsakis A, Tzanakakis G, et al. HA metabolism in skin homeostasis and inflammatory disease. Food Chem Toxicol 2017;101:128–38.

Kishibe M, Bando Y, Tanaka T, Ishida-Yamamoto A, Iizuka H, Yoshida S. Kallikrein-related peptidase 8-dependent skin wound healing is associated with upregulation of kallikrein-related peptidase 6 and PAR2. J Invest Dermatol 2012;132:1717–24.

Kobayashi T, Chanmee T, Itano N. Hyaluronan: metabolism and function. Biomolecules 2020;10:1525.

Lee MJ, Kim DH, Ryu JS, Ko AY, Ko JH, Kim MK, et al. Topical TSG-6 administration protects the ocular surface in two mouse models of inflammation-related dry eye. Invest Ophthalmol Vis Sci 2015;56:5175–81.

Lee TH, Lee GW, Ziff EB, Vilcek J. Isolation and characterization of eight tumor necrosis factor-induced gene sequences from human fibroblasts. Mol Cell Biol 1990;10:1982–8.

Lesley J, Gál I, Mahoney DJ, Cordell MR, Rugg MS, Hyman R, et al. TSG-6 modulates the interaction between hyaluronan and cell surface CD44. J Biol Chem 2004;279:25745–54.

Lin W, Shuster S, Maibach HI, Stern R. Patterns of hyaluronan staining are modified by fixation techniques. J Histochem Cytochem 1997;45:1157–63.

Livak KJ, Schmittgen TD. Analysis of relative gene expression data using real-time quantitative PCR and the 2(−Delta Delta C(T)) method. Methods 2001;25:402–8.

Malaisse J, Bourguignon V, De Vuyst E, Lambert de Rouvroit C, Nikkels AF, Flamion B, et al. Hyaluronan metabolism in human keratinocytes and atopic dermatitis skin is driven by a balance of hyaluronan synthases 1 and 3. J Invest Dermatol 2014;134:2174–82.

Mathay C, Pierre M, Pittelkow MR, Depiereux E, Nikkels AF, Colige A, et al. Transcriptional profiling after lipid raft disruption in keratinocytes identifies critical mediators of atopic dermatitis pathways. J Invest Dermatol 2011;131:46–58.

Meyer LJ, Stern R. Age-dependent changes of hyaluronan in human skin. J Invest Dermatol 1994;102:385–9.

Milner CM, Day AJ. TSG-6: a multifunctional protein associated with inflammation. J Cell Sci 2003;116:1863–73.

Milner CM, Tongsoongnoen W, Rugg MS, Day AJ. The molecular basis of inter-alpha-inhibitor heavy chain transfer on to hyaluronan. Biochem Soc Trans 2007;35:672–6.

Minner F, Herphelin F, Poumay Y. Study of epidermal differentiation in human keratinocytes cultured in autocrine conditions. Methods Mol Biol 2010;585:71–82.

Minner F, Poumay Y. Candidate housekeeping genes require evaluation before their selection for studies of human epidermal keratinocytes. J Invest Dermatol 2009;129:770–3.

Moran MC, Pandya RP, Leffler KA, Yoshida T, Beck LA, Brewer MG. Characterization of human keratinocyte cell lines for barrier studies. JID Innov 2021;1:100018.

Morioka Y, Yamasaki K, Leung D, Gallo RL. Cathelicidin antimicrobial peptides inhibit hyaluronan-induced cytokine release and modulate chronic allergic dermatitis. J Immunol 2008;181:3915–22.

Mound A, Lozanova V, Warnon C, Hermant M, Robic J, Guere C, et al. Non-senescent keratinocytes organize in plasma membrane submicrometric lipid domains enriched in sphingomyelin and involved in re-epithelialization. Biochim Biophys Acta Mol Cell Biol Lipids 2017;1862:958–71.

Muto J, Sayama K, Gallo RL, Kimata K. Emerging evidence for the essential role of hyaluronan in cutaneous biology. J Dermatol Sci 2019;94:190–5.

Nauroy P, Nyström A. Kallikreins: essential epidermal messengers for regulation of the skin microenvironment during homeostasis, repair and disease. Matrix Biol Plus 2020;6–7:100019.

Park AY, Bourtembourg M, Chrétien A, Hubaux R, Lancelot C, Salmon M, et al. Modulation of gene expression in a sterile atopic dermatitis model and inhibition of *Staphylococcus aureus* adhesion by fucoidan. Dermatopathology (Basel) 2021;8:69–83.

Pasonen-Seppänen S, Hyttinen JM, Rilla K, Jokela T, Noble PW, Tammi M, et al. Role of CD44 in the organization of keratinocyte pericellular hyaluronan. Histochem Cell Biol 2012;137:107–20.

Pasonen-Seppänen S, Karvinen S, Törrönen K, Hyttinen JM, Jokela T, Lammi MJ, et al. EGF upregulates, whereas TGF-beta downregulates, the hyaluronan synthases Has2 and Has3 in organotypic keratinocyte cultures: correlations with epidermal proliferation and differentiation. J Invest Dermatol 2003;120:1038–44.

Perez A, Neskey DM, Wen J, Pereira L, Reategui EP, Goodwin WJ, et al. CD44 interacts with EGFR and promotes head and neck squamous cell carcinoma initiation and progression. Oral Oncol 2013;49:306–13.

Plager DA, Kahl JC, Asmann YW, Nilson AE, Pallanch JF, Friedman O, et al. Gene transcription changes in asthmatic chronic rhinosinusitis with nasal polyps and comparison to those in atopic dermatitis. PLoS One 2010;5:e11450.

Quaranta M, Knapp B, Garzorz N, Mattii M, Pullabhatla V, Pennino D, et al. Intraindividual genome expression analysis reveals a specific molecular signature of psoriasis and eczema. Sci Transl Med 2014;6:244ra90.

Reynolds G, Vegh P, Fletcher J, Poyner EFM, Stephenson E, Goh I, et al. Developmental cell programs are co-opted in inflammatory skin disease. Science 2021;371:eaba6500.

Rheinwald JG, Hahn WC, Ramsey MR, Wu JY, Guo Z, Tsao H, et al. A two-stage, p16(INK4A)- and p53-dependent keratinocyte senescence mechanism that limits replicative potential independent of telomere status. Mol Cell Biol 2002;22:5157–72.

Rosdy M, Pisani A, Ortonne JP. Production of basement membrane components by a reconstructed epidermis cultured in the absence of serum and dermal factors. Br J Dermatol 1993;129:227–34.

Sakai S, Yasuda R, Sayo T, Ishikawa O, Inoue S. Hyaluronan exists in the normal stratum corneum. J Invest Dermatol 2000;114:1184–7.

Sandjeu Y, Haftek M. Desmosealin and other components of the epidermal extracellular matrix. J Physiol Pharmacol 2009;60(Suppl. 4):23–30.

Selbi W, Day AJ, Rugg MS, Fülöp C, de la Motte CA, Bowen T, et al. Overexpression of hyaluronan synthase 2 alters hyaluronan distribution and function in proximal tubular epithelial cells. J Am Soc Nephrol 2006;17:1553–67.

Shakya S, Mack JA, Alipour M, Maytin EV. Cutaneous wounds in mice lacking TSG-6 exhibit delayed closure and an abnormal inflammatory response. J Invest Dermatol 2020;140:2505–14.

Simpson RM, Meran S, Thomas D, Stephens P, Bowen T, Steadman R, et al. Age-related changes in pericellular hyaluronan organization leads to impaired dermal fibroblast to myofibroblast differentiation. Am J Pathol 2009;175:1915–28.

Smits JPH, Niehues H, Rikken G, van Vlijmen-Willems IMJJ, van de Zande GWHJF, Zeeuwen PLJM, et al. Immortalized N/TERT keratinocytes as an alternative cell source in 3D human epidermal models. Sci Rep 2017;7:11838.

Tammi RH, Tammi MI, Hascall VC, Hogg M, Pasonen S, MacCallum DK. A preformed basal lamina alters the metabolism and distribution of hyaluronan in epidermal keratinocyte "organotypic" cultures grown on collagen matrices. Histochem Cell Biol 2000;113:265–77.

Tan KT, McGrouther DA, Day AJ, Milner CM, Bayat A. Characterization of hyaluronan and TSG-6 in skin scarring: differential distribution in keloid scars, normal scars and unscarred skin. J Eur Acad Dermatol Venereol 2011;25:317–27.

Tan Q, Thomassen M, Burton M, Mose KF, Andersen KE, Hjelmborg J, et al. Generalized correlation coefficient for non-parametric analysis of microarray time-course data. J Integr Bioinform 2017;14:20170011.

Toole BP. Hyaluronan in morphogenesis. Semin Cell Dev Biol 2001;12:79–87.

Toole BP. Hyaluronan: from extracellular glue to pericellular cue. Nat Rev Cancer 2004;4:528–39.

Wang F, Flanagan J, Su N, Wang LC, Bui S, Nielson A, et al. RNAscope: a novel in situ RNA analysis platform for formalin-fixed, paraffin-embedded tissues. J Mol Diagn 2012;14:22–9.

Weigel PH, Hascall VC, Tammi M. Hyaluronan synthases. J Biol Chem 1997;272:13997–4000.